Bull Earthquake Eng (2014) 12:875–908
DOI 10.1007/s10518-013-9538-0

ORIGINAL RESEARCH PAPER

The rocking response of large flexible structures to earthquakes

Sinan Acikgoz · Matthew J. DeJong

Received: 27 October 2012 / Accepted: 10 October 2013 / Published online: 5 November 2013

Abstract The rocking response of structures subjected to strong ground motions is a problem of 'several scales'. While small structures are sensitive to acceleration pulses acting successively, large structures are more significantly affected by coherent low frequency components of ground motion. As a result, the rocking response of large structures is more stable and orderly, allowing effective isolation from the ground without imminent danger of overturning. This paper aims to characterize and predict the maximum rocking response of large and flexible structures to earthquakes using an idealized structural model. To achieve this, the maximum rocking demand caused by different earthquake records was evaluated using several ground motion intensity measures. Pulse-type records which typically have high peak ground velocity and lower frequency content caused large rocking amplitudes, whereas non-pulse type records caused random rocking motion confined to small rocking amplitudes. Coherent velocity pulses were therefore identified as the primary cause of significant rocking motion. Using a suite of pulse-type ground motions, it was observed that idealized wavelets fitted to velocity pulses can adequately describe the rocking response of large structures. Further, a parametric analysis demonstrates that pulse shape parameters affect the maximum rocking response significantly. Based on these two findings, a probabilistic analysis method is proposed for estimating the maximum rocking demand to pulse-type earthquakes. The dimensionless demand maps, produced using these methods, have predictive power in the near-field provided that pulse period and amplitude can be estimated a priori. Use of this method within a probabilistic seismic demand analysis framework is briefly discussed.

Keywords Rocking · Uplift · Near-field ground motion · Dimensional analysis · Probabilistic seismic demand analysis · Earthquake engineering

S. Acikgoz (✉) · M. J. DeJong
Department of Engineering, University of Cambridge, Trumpington Street, Cambridge CB2 1PZ, UK
e-mail: msa44@cam.ac.uk; msinanacikgoz@gmail.com

M. J. DeJong
e-mail: mjd97@cam.ac.uk

1 Introduction

Independent analytical and experimental works have repeatedly shown the sensitivity of rigid rocking motion to various system parameters. It has been reported that small changes in size, slenderness or ground motion may result in drastic changes in rocking response (e.g. Aslam et al. 1980). This sensitive dynamic behavior has led to the conclusion that the response is random and systematic trends can only be observed when the problem is studied from a probabilistic perspective (Yim et al. 1980; Sorrentino et al. 2006; DeJong 2012).

Makris and Roussos (2000) have argued that the randomness of the response can be partially attributed to the fact that the ground motions utilized in earlier studies had no coherent components. Rocking amplification was therefore the result of the interaction of a number of random impulses. However, they suggested that the hidden low frequency velocity pulses in earthquakes are the primary driving forces of large rocking motion. Their analyses further showed that acceleration pulses can override the coherent pulse and can significantly amplify the response. In general, shorter acceleration pulses have a larger effect on smaller structures, which have less resistance to rocking. Larger rocking structures, which have higher resistance, are less affected. This behavior stems from the 'scale effect' mentioned by Housner (1963), which suggests that the effect of a pulse on response is determined by the pulse frequency relative to the structural size. Therefore, the earthquake response of rigid rocking structures is a problem of 'several scales'; while the relative effect of shorter duration acceleration pulses may be definitive for small structures, large structures may be primarily affected by the longer duration coherent pulses.

This paper is concerned with the rocking response of large structures to strong ground motion. Previous research has largely been motivated by the rocking exhibited by smaller rigid structures (e.g. electric transformers, tombstones) with a strong focus on overturning (see Zhang and Makris 2001 and references therein). However, numerous large structures were observed to exhibit rocking during earthquakes without overturning, such as elevated water tanks and slender towers (Yim et al. 1980). Experimental and analytical research to follow indicated that rocking isolates the structure from the ground, limiting the inertial forces as a result of earthquake motion while sustaining large displacements without residual damage (Meek 1975; Huckelbridge and Clough 1978). In New Zealand, a bridge and an industrial chimney have been designed to rock during strong ground motion to benefit from base isolation effects (Beck and Skinner 1973; Sharpe and Skinner 1983).

For larger scale structures flexibility must inherently be considered. Therefore rocking structures may have variable size and flexibility, and previous work by the authors quantifies the effects of these parameters on the rocking response (Acikgoz and DeJong 2012). To address this wide variety of structures, an idealized flexible rocking structure model is used (see Fig. 1). This lumped mass analytical model may be a direct representation of single-stem bridges or elevated water tanks where significant mass is lumped at a height. Previous research has suggested that the response of similar models is also relevant in the investigation of more complicated structures (Meek 1978; Psycharis 1983; Yim and Chopra 1985). In order to explore some general trends of the earthquake response of rocking structures, the analytical model investigates an idealized rigid-rigid contact. While notable investigations have been carried out considering interface compliance (Psycharis 1983; Yim and Chopra 1984a,b, 1985), such compliance is not considered here because it is structure specific and its implementation requires a meticulous consideration of interface materials and detailing.

The focus of this investigation is on determining the maximum rocking response. Initially, the aim is to characterize the earthquake response of large flexible rocking structures by identifying factors that induce high rocking amplitudes. To achieve this objective, an attempt

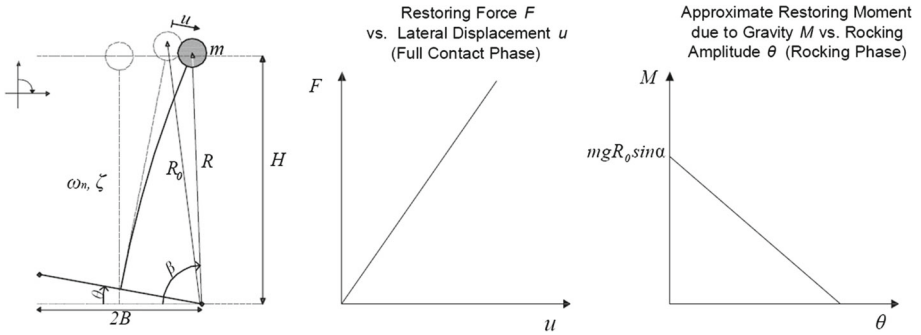

Fig. 1 Schematic of the idealized analytical model of a flexible rocking structure (*left*), the corresponding force-displacement relationship during the full contact phase (*middle*), and the corresponding approximate restoring moment -rotation diagram during the rocking phase (*right*)

will be made to correlate simple intensity measures (IMs) to maximum rocking demand. Realizing that coherent velocity pulses may be the primary cause of large rocking action, attention is focused on pulse-type records. While both trigonometric pulses and wavelets have been proposed to idealize earthquake records (e.g. Apostolou et al. 2007), wavelets have been shown to thoroughly represent the salient characteristics of coherent velocity pulses (Vassiliou and Makris 2011), and therefore have the potential to be utilized, in lieu of pulse-type records, in structural design and analysis (Mavroeidis et al. 2004; Sehhati 2008). Therefore, to systematically investigate the role of pulses in the response, the wavelet formulation proposed by Mavroeidis and Papageorgiou (2003) is utilized in this study.

After evaluating the ability of wavelets to capture the rocking response, the focus progresses to predicting rocking response during pulse-type earthquakes. In particular, the use of wavelets to produce dimensionless demand maps, which can estimate the rocking demand for a complete range of realistic velocity pulses and structural size parameters, is investigated. The use of such maps within a probabilistic framework is then considered, the goal being to predict the probability of exceedance of the maximum rocking amplitude above a specified design limit. The extension of this framework to non-pulse type earthquakes, the response to which is demonstrated to be largely probabilistic, is briefly discussed.

2 Brief review of the structural model

To evaluate the earthquake response of large and flexible rocking structures, it is useful to briefly review the structural model employed (see Acikgoz and DeJong 2012 for further detail concerning the model and Acikgoz and DeJong 2013 for an experimental validation). The model (Fig. 1, left) consists of a point mass m on an axially rigid strut connected to a rigid foundation beam. The height of the structure is H, the base width is $2B$ and the slenderness is $\alpha = \tan^{-1}(B/H)$. The structure is allowed to rock while deforming elastically. The parameter u is the elastic translation of the mass and θ is the rigid body rotation of the foundation.

Before uplift, the structure responds identically to a typical single degree of freedom oscillator. This phase of motion is defined as the full contact phase. The response is characterized by the natural frequency ω_n and damping ratio ζ. The constant positive stiffness observed during this phase is illustrated in Fig. 1 (middle).

Upon uplift, rocking commences alongside elastic translation. The exact equations of motion of the rocking phase, describing the elastic translation and rocking, were derived in Acikgoz and DeJong (2012) using the generalized coordinates (R, β) and in Acikgoz and

DeJong (2013) using (u, θ). These generalized coordinates are illustrated in Fig. 1 (left). For the sake of clarity, only the (u, θ) set of coordinates are used herein, for which the equations of motions are:

$$\ddot{u} + H\ddot{\theta} + (\pm B - u)\dot{\theta}^2 + 2\zeta\omega_n\dot{u} + \omega_n^2 u = -\ddot{u}_g \cos\theta + g\sin\theta \tag{1a}$$

$$\left(R_0^2 + u^2 \mp 2Bu\right)\ddot{\theta} + H\ddot{u} \mp 2\dot{\theta}\dot{u}(B \mp u) = +\ddot{u}_g\left(-R_0\cos(\alpha \mp \theta) + u\sin\theta\right) + g\left(\mp R_0\sin(\alpha \mp \theta) + u\cos\theta\right) \tag{1b}$$

where $R_0 = \sqrt{H^2 + B^2}$ is the distance between the lumped mass and the base pivot when $u = 0$. Gravitational and ground motion accelerations are denoted by g and $\ddot{u}_g$ (dots refer to differentiation with respect to time) respectively. An additional relevant term $p = \sqrt{g/R_0}$ is the frequency parameter, an important indicator of the scale of the structure. In Eq. 1, the upper sign denotes rocking about the right base corner and the lower sign about the left base corner.

Algebraic manipulations of the coupled nonlinear expressions in Eq. 1 demonstrate that once uplifted, the vibration characteristics of the system are altered significantly (Acikgoz and DeJong 2013). The oscillation frequency and damping significantly increase with the initiation of rocking when $R_0 >> B$, and inertial elastic forces counteract rocking. However, when the elastic motion is damped out, Eq. 1b becomes quite similar to the rigid rocking equation of motion (e.g. Housner 1963), suggesting that flexible rocking structures show similar moment-rotation behavior to rigid rocking structures (Acikgoz and DeJong 2012). This moment rotation behavior is characterized by negative stiffness and scale dependence (see Fig. 1, right). The fact that different stiffness characteristics are observed during different phases of motion is important, as it suggests that different structural behavior may be significant in causing uplift versus amplifying rocking response.

The transition between different phases of motion is accompanied by energy dissipation due to radiation damping. For brevity, the details of transition are not discussed here. The interested reader is referred to Acikgoz and DeJong (2012), where details about the numerical simulation of the equations of motion in MATLAB (Mathworks, Natick, MA) can also be found.

3 Characterizing the rocking response

3.1 Rocking response to earthquake records

3.1.1 Time history response

To investigate the effect of pulse-type earthquakes on building frame structures, Anderson and Bertero (1987) utilized near-field earthquake records from the 1979 Imperial Valley Earthquake. Due to fault rupture characteristics and station locations, some records include a velocity pulse while the others do not. A similar approach is adopted in this section to investigate the response of a large and flexible rocking structure, though the earthquake records are not identical.

In this paper, a large structure is defined as a structure which has a frequency parameter $p \leq$ 1rad/s. To put this value into perspective with respect to other rocking structures mentioned in previous studies: $p \approx 3.5$ rad/s for a typical tombstone, $p \approx 2$ rad/s for an electric transformer (Zhang and Makris 2001), $p \approx 1.5$ rad/s for a classical monolithic column

Table 1 Earthquake events considered in this study

Event ID	Earthquake	Year	M_w	Event ID	Earthquake	Year	M_w
IV40	Imperial Valley	1940	7.0	NA	Nahanni	1985	6.8
SF	San Fernando	1971	6.6	NP	North Palm Springs	1986	6.1
BU	Bucharest	1977	7.5	SH	Superstition Hills	1987	6.5
TA	Tabas	1978	7.4	LP	Loma Prieta	1989	6.9
CL	Coyote Lake	1979	5.7	CM	Cape Mendocino	1992	7.0
IV79	Imperial Valley	1979	6.5	LA	Landers	1992	7.3
IR	Irpinia	1980	6.9	NO	Northridge	1994	6.7
MH	Morgan Hill	1984	6.2	CH	Chi Chi	1999	7.6

(Makris and Vassiliou 2012) and p is typically less than 1 rad/s for bridge piers (e.g. Beck and Skinner 1973) or relatively tall building frame structures (e.g. Huckelbridge and Clough 1978). For this initial investigation, a slender structure with $\alpha \approx 0.15$ rad and frequency parameter $p = 1$ rad/s was chosen. This corresponds to a structural geometry with base width 2.94 m and height 9.7 m. A natural frequency of $\omega_n = 10$ rad/s and a damping ratio of $\zeta = 0.05$ were specified. These slenderness and damping ratio values will be utilized throughout the paper. It should be noted that due to the specified slenderness, low energy dissipation is typically expected at impacts.

Near-field earthquake time histories from Bonds Corner station and the EC Diff Array, both recorded during the 1979 Imperial Valley Earthquake (identified as event 'IV79' in Table 1), were selected for initial investigation. The acceleration and velocity time histories from these records are shown in Fig. 2 and their IMs are presented in Table 2. The record from Bonds Corner station, 2.7 km away from the causative fault, has high peak ground acceleration (PGA = 0.77 g), long significant duration (Trifunac and Brady 1975) and maximum frequency content approximately at the natural frequency ω_n. A high peak ground velocity (PGV) of 0.46 m/s is observed, indicating significant low frequency content. The record from the EC Diff Array, located 7 km away from the causative fault, has a much smaller PGA of 0.35 g, a shorter significant duration and lesser frequency content at the natural frequency ω_n. However, it has a PGV of 0.71 m/s and a forward directivity pulse is evident in its velocity time history.

Figure 2 presents the rocking and elastic deformation response of the flexible rocking structure under consideration. The elastic deformation of a linear elastic oscillator with similar properties is also provided for comparison. As expected, the response of the linear elastic oscillator to the Bonds Corner record is very large due to elastic amplification (Fig. 2, bottom row). The flexible rocking structure behaves identically to a linear elastic oscillator before uplift, but elastic deformation due to resonance effects is limited once rocking initiates, and does not lead to large rocking motion. Instead, repeated uplift cycles are observed; the relatively high frequency acceleration pulses which induce uplift do not sustain rocking motion. However, significant maximum rocking amplitude is observed due to interaction of several pulses around $t = 9$ s. Larger rocking is observed in the EC Diff Array record for a much smaller PGA. The smooth response indicates that rocking is governed by the coherent pulse, and is largely unaffected by the high frequency oscillation. Upon the termination of the pulse, the rocking action dies away. Pulses do not seem to illicit an increased elastic response. Effective base isolation can be observed in both cases as the elastic deformations excited during impact are quickly damped out and ground motion seems to have negligible influence on ensuing elastic deformation behaviour.

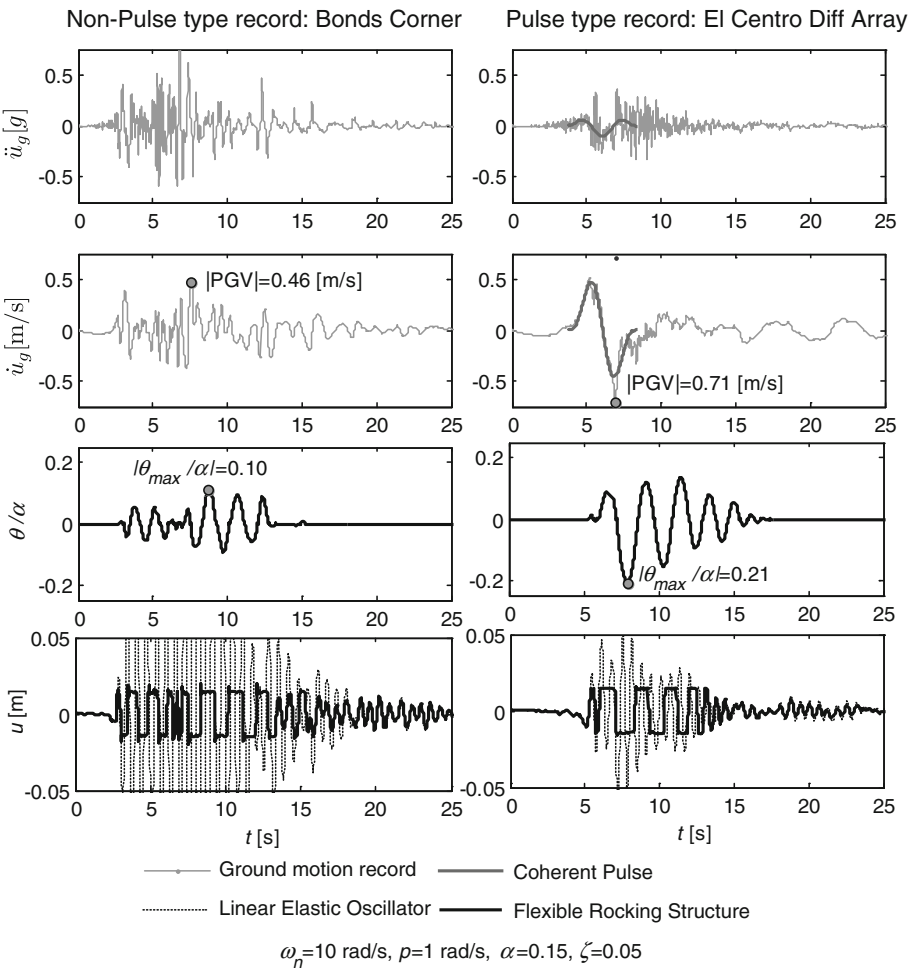

Fig. 2 Acceleration (*top row*) and velocity (2nd *row*) time histories of the non-pulse type Bonds Corner (*left column*) and pulse-type EC Diff Array (*right column*) records, followed by the rocking (3rd *row*) and elastic deformation (4th *row*) responses of a flexible rocking structure to these records

Figure 2 illustrates the different rocking amplification mechanisms observed in non-pulse and pulse-type earthquakes. For the non-pulse type record, amplification occurs as a result of the interaction of different acceleration pulses, and rocking action is confined to smaller amplitudes. The response to the pulse-type earthquake is more orderly as it is largely controlled by a single coherent velocity pulse which generates more rocking. To generalize these results, the rocking spectra resulting from numerous pulse-type and non-pulse type earthquakes are evaluated in the following sections.

3.1.2 Spectral response

Analogous to a typical displacement response spectrum, a rocking spectrum can be used to present the maximum rocking response with respect to the natural frequency of the structure. Figure 3 shows the rocking demand experienced by the structure specified in Sect. 3.1.1

Table 2 Ground motion IMs of nine pulse-type and nine non-pulse type records and their associated SDM

Event ID	Station (component)	D^{a} [km]	Ground motion intensity measures							Spectral demand measure, SDM[g]
			Acceleration based [g]		Velocity based [m/s]		Period based [s]			
			PGA	$\bar{a}^{b}$	MIV[c]	PGV	T_m^{d}	T_{vs}^{e}	T_p^{f}	
(a) Pulse-type records										
CH	TCU 052 (FN)	0.2	0.35	0.11	1.37	1.59	1.57	2.20	7.91	1.000
SH	Parachute test site (FN)	0.7	0.46	0.16	1.99	1.12	1.11	1.80	2.06	0.890
NO	New Hall Pico C Rd. (FN)	7.1	0.45	0.17	1.81	0.93	1.56	2.20	3.46	0.716
BU	Bucharest (NS)	115	0.20	0.09	1.19	0.74	1.63	1.75	1.88	0.410
SF	Pacoima Dam (FN)	2.8	1.23	0.27	1.13	1.12	0.48	1.55	1.54	0.349
NP	N. Palm Springs (FN)	8.2	0.59	0.16	0.52	0.73	0.61	1.05	1.37	0.224
MH	Coyote Lake Dam (FN)	0.1	0.71	0.22	0.73	0.52	0.42	0.65	1.09	0.141
IV79	EC diff. array (FN)	7	0.35	0.14	0.64	0.71	0.50	4.40	5.75	0.090
NA	Site 2 (FP)	8.0	0.32	0.08	0.28	0.33	0.40	0.55	0.9	0.040
Average			0.52			0.87			2.88	0.429
Kendall rank correlation coefficient b/w IM & SDM			0.03	0.08	0.78	0.82	0.61	0.53	0.61	
(b) Non-pulse type records										
CH	CHY080 (FP)	2.7	0.90	0.20	1.62	1.02	0.85	0.85	1.95	0.51
IV79	Bonds Corner (FN)	2.7	0.77	0.19	0.84	0.46	0.46	0.55	1.84	0.153
NA	Site 1 (FN)	5.3	1.10	0.17	0.61	0.46	0.35	0.30	1.56	0.118
SH	Spst Mtn Camera (FP)	4.3	0.89	0.18	0.50	0.42	0.38	0.75	0.86	0.098
IV40	El Centro (NS)	8.3	0.32	0.07	0.42	0.36	0.53	0.85	1.92	0.077
NO	Century CC North (FP)	25.7	0.26	0.08	0.27	0.21	0.51	0.60	0.92	0.054
NP	Whitewater Trout F(FN)	7.3	0.49	0.19	0.52	0.35	0.35	0.55	0.64	0.047

Table 2 continued

Event ID	Station (component)	D^{a} [km]	Ground motion intensity measures							Spectral demand measure, SDM[g]
			Acceleration based [g]		Velocity based [m/s]		Period based [s]			
			PGA	$\bar{a}^{b}$	MIV[c]	PGV	T_m^{d}	T_{vs}^{e}	T_p^{f}	
MH	Anderson Dam (FP)	2.6	0.29	0.11	0.45	0.28	0.56	0.7	1.01	0.045
SF	Castaic (FP)	22.6	0.32	0.06	0.25	0.16	0.36	0.35	0.84	0.019
Average			0.59			0.41			1.28	0.125
Kendall rank correlation coefficient b/w IM&SDM			0.54	0.54	0.72	0.87	0.14	0.23	0.56	

FN fault normal, *FP* fault parallel, *NS* North-South

[a] Closest distance to the fault plane (Abrahamson and Silva 1997); [b] Root mean squared acceleration; [c] Maximum Incremental Velocity (Anderson and Bertero 1987); [d] Mean period (Rathje et al. 1998); [e] Period corresponding to velocity spectrum maximum (Baker 2007); [f] Velocity pulse period (Bray and Rodriguez-Marek 2004); [g] see Eq. 2

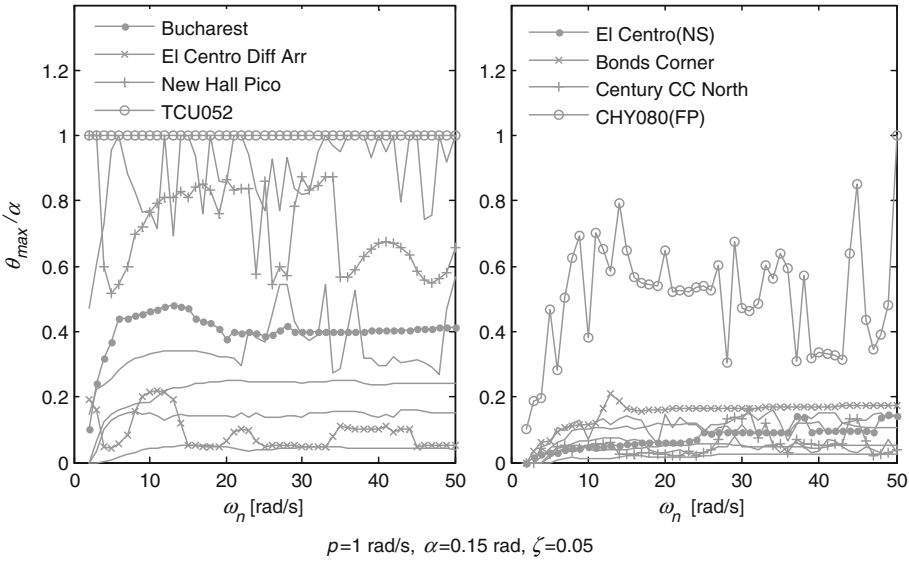

Fig. 3 Rocking spectra for a flexible rocking structure subjected to the nine pulse-type records (*left*) and nine non-pulse type records (*right*) listed in Table 2. Note that the legend is not comprehensive

under the influence of nine pulse-type records and nine non-pulse type records from the earthquakes listed in Table 1. With the exception of the Bucharest record, pulse-type records have been identified among those in Baker (2007). The IMs associated with the records are presented in Table 2. Seven of the pulse-type records feature directivity pulses, one has a pulse in the fault parallel direction, and one is a far-field record with a pulse caused by local geologic effects. Eight of the non-pulse type records are from the near-field and one is from the far-field. More near-field non-pulse type records were selected as they often have a richer low frequency content which is potentially hazardous for rocking structures.

To determine the destructiveness of a record for a structure with given geometry (p, α) and damping (ζ) over a range of natural frequencies, a spectral demand measure (SDM) is defined. This parameter compares the area under the rocking spectrum for a given earthquake record with the area under the rocking spectrum of a hypothetical record which causes overturning for the whole range of natural frequencies. When the maximum rocking angle exceeds the slenderness angle the ordinate of the rocking spectrum is assumed to obtain a value of $\theta/\alpha = 1$. It is recognized that the maximum rocking increases without bound when overturning occurs and that the rocking angle may exceed the slenderness angle without overturning. However, as the primary focus of this paper is assessing the exceedance of maximum rocking/SDM levels less than $\theta = \alpha$, differentiating between overturning and the relatively rare event of recovery after θ exceeds α is statistically insignificant. The following expression was used to define SDM values for the spectra presented in Fig. 3:

$$\mathrm{SDM} = \frac{1}{\omega_{nf} - \omega_{n0}} \int_{\omega_{n0}}^{\omega_{nf}} \frac{\theta_{\max}}{\alpha} d(\omega_n) \tag{2}$$

where ω_{nf} and ω_{n0} are the upper and lower bound natural frequencies of the considered spectra ($\omega_{n0} = 2$ rad/s and $\omega_{nf} = 50$ rad/s are used in this case).

The comparison of responses in Fig. 3 clearly indicates that pulse-type records induced larger rocking amplitudes despite having similar average PGAs. In fact, for the considered structure, rocking caused by non-pulse type earthquakes was typically limited to around 0.1α, with the exception of the CHY080 record which has an exceptionally high PGV for a non-pulse type record. It is important to highlight the response to the pulse-type TCU052 record from the same earthquake, which caused rocking angles in excess of the slenderness for all structural configurations investigated. In addition, Fig. 3 indicates that the rocking response to all earthquakes can be sensitive to small changes in flexibility. For non-pulse type earthquakes, the response caused by two of the four records highlighted in the legend show particular sensitivity to the natural frequency of the structure. For pulse-type earthquakes significant sensitivity is typically observed for records which induce high rocking amplitudes due to low resistance to rocking at these amplitudes.

In Table 2, the records are ordered according to decreasing SDM. For non-pulse type records, many of the IMs do not correlate well with the SDM. This can be demonstrated using the Kendall rank correlation coefficient, which quantifies the 'association' between the IMs and the corresponding SDM for pulse-type and non-pulse type data sets. PGV and MIV yield the highest rank correlations for the non-pulse type data set because these parameters indicate the presence of low frequency acceleration pulses interacting with each other to amplify rocking (Sorrentino et al. 2006). The correlation may have been better if higher radiation damping was specified, limiting the interaction between pulses (DeJong 2012). However, the structures utilized throughout the paper are slender and are therefore characterized by relatively little radiation damping. Despite the small size of the data set used in the evaluation, Fig. 3 generally confirms that the rocking response to non-pulse type records should be evaluated probabilistically (Yim et al. 1980).

The rocking spectra of pulse-type records in Fig. 3 (left) depict a large variability in the response to different records. As a similar variability is not observed for non-pulse type excitations, this variability is likely related to pulse characteristics. Therefore, IMs which describe the period and amplitude of velocity pulses should correlate better with the SDM. The acceleration based IMs considered are the PGA and the root mean squared acceleration $\bar{a}$. These measures are significantly influenced by acceleration pulses and therefore are not good indicators of velocity pulse characteristics. Similarly, the maximum incremental velocity (MIV) is a measure pertaining to large acceleration pulses (Anderson and Bertero 1987). PGV, on the other hand, is less influenced by acceleration pulses, and could therefore be used as an indicator of the pulse amplitude. Several definitions exist for defining the dominant pulse period. The mean period T_m, as defined by Rathje et al. (1998), is a weighted average of all the frequencies observed in the frequency domain of an earthquake record. Another common indicator is the period T_{vs} at which the elastic velocity response spectrum reaches its maximum value (e.g. Baker 2007). Alternatively, the pulse period T_p as proposed by Bray and Rodriguez-Marek (2004), assumes that the period of the largest amplitude velocity pulse half cycle represents the dominant pulse period. Amongst these definitions, only the definition of Bray and Rodriguez-Marek (2004) relates unambiguously to the velocity pulse period. The mean period and the pulse period estimated from the velocity spectrum are influenced by non-pulse components of earthquakes and therefore may underestimate the velocity pulse period.

The accuracy of PGV and T_p in estimating pulse amplitude and velocity will be investigated later (see Sect. 3.2.3). However, assuming that these parameters are good indicators, comparing them to the SDM provides valuable insight. For pulse type records, the values of T_p typically decrease with the SDM, with the exception of the EC Diff Array and New Hall Pico C. Rd. records. The unexpected behavior of the EC Diff Array record, which has the

second highest pulse period but one of the lowest SDMs, can be explained by the inadequate amplitude of its velocity record. The pulse within this record has an associated acceleration peak which barely causes uplift for a wide range of structural frequencies and therefore cannot sustain rocking motion. PGV has the highest rank correlation coefficient for the pulse-type earthquake data set although the Pacoima Dam and Superstition Hills records with identical PGVs result in significantly different SDM values.

In summary, greater rocking response was facilitated, at least in part, by coherent velocity pulses. Simple ground motion IMs could not be directly correlated to rocking demand and certain records (e.g. EC Diff Array) indicate that the response to pulse-type earthquakes is not straightforward. Furthermore, fluctuations in the response to the New Hall Pico C. Rd. record (Fig. 3, left) indicate that acceleration pulses may also affect the response. Based on these observations, the following sections focus on better quantifying the effect of velocity pulses, idealized using wavelets, on the rocking response.

3.2 Categorization of pulses

3.2.1 Selection of ground motion records

To assess the vulnerability of rocking structures pulse-type earthquakes, a suite of records was selected from a list of ground motion records identified as pulse-type by Baker (2007). The records are presented in Table 3 with their salient seismological parameters. With the exception of the Bucharest record from the IESD database (Ambraseys et al. 2004), all of the chosen records are from the near-field (closest distance to the fault plane, $D < 25$ km) and were obtained from the PEER NGA database (Chiou et al. 2008). They all have a moment magnitude (M_w) greater than 5.5 and a PGV greater than 0.3 m/s. The records are from a variety of different geological sites including rock and soft soil conditions. Unless specified, all of the records are fault normal (FN) components of ground motion, although a number of fault parallel (FP) records have also been included.

3.2.2 Determining pulse parameters

The pulse-type records feature a dominating single velocity pulse with a relatively simple form. It is desirable to have a mathematical expression that unambiguously addresses the pulse period and amplitude, and the number and phase of half-cycles. One such pulse form was proposed by Mavroeidis and Papageorgiou (2003), which will be utilized in this investigation and will be referred to as the M&P wavelet.

The M&P wavelet is an amplitude modulated harmonic. It is described as follows:

$$\dot{u}_p = \begin{cases} \frac{A}{2}\left[1+\cos\left(\frac{\omega}{\gamma}(t-t_0)\right)\right]\cos\left(\omega(t-t_0)+\phi\right), & t_0-\frac{\pi\gamma}{\omega} < t < t_0+\frac{\pi\gamma}{\omega} \\ 0 & \text{otherwise} \end{cases} \tag{3}$$

where A controls the amplitude of the velocity signal, ω determines the dominant frequency of the wavelet, γ controls the number of half cycles and ϕ is the phase of the harmonic. Additionally, t_0 indicates the epoch of the envelope and allows the translation of the pulse along the time axis. The M&P wavelet is not a single frequency function. The period of the wavelet, defined by Mavroeidis and Papageorgiou (2003) as $T = 2\pi/\omega$, is therefore only an approximate measure of the dominant pulse period.

A nonlinear least squares fitting procedure was implemented in MATLAB (Mathworks, Natick, MA) to determine the pulse parameters. The automated procedure requires initial

Table 3 Relevant seismological parameters for the pulse-type ground motion records considered in this study, and corresponding M&P wavelet fit parameters (see Sect. 3.2.2)

Bin[a]	ID	Station (component)	D [km]	|PGV| [m/s]	T_p [s]	A [m/s]	ω [rad]	γ	Φ	E_p	E_{th}
1B	NO	Rinaldi	7.1	1.60	1.32	1.76	4.69	1	1.07	0.01	0.66
1B	LA	Lucerne	1.1	1.47	10.51	1.42	0.82	0.86	1.08	0.06	0.9
1B	MH	Coyote Lake Dam	0.1	0.52	1.09	−0.71	5.08	0.81	1.22	0.04	0.54
1C	IV79	EC Diff Array	5.3	0.71	4.69	0.71	1.40	1.02	1.54	0.12	0.72
1C	IV79	Brawley Airport	8.5	0.36	2.81	0.48	1.27	0.84	1.62	0.06	0.61
1C	NO	New Hall Pico C Rd.	7.1	0.93	2.69	−1.32	2.38	1.06	1.66	0.06	0.85
1C	IV79	EC Array #10	8.6	0.48	4.6	−0.59	1.41	1	1.80	0.06	0.59
1D	NA	Site 2	8.0	0.33	0.9	−0.33	6.97	1.19	2.85	0.02	0.48
2A	SF	Pacoima Dam	2.8	1.13	1.54	−1.03	4.04	1.45	3.08	0.05	0.5
2A	CH	TCU052	0.2	1.59	7.24	1.35	0.85	1.73	0.21	0.32	0.7
2B	CH	TCU076	2.0	0.63	3.69	−0.45	1.67	1.71	0.59	0.25	0.42
2C	SH	Parachute Test Site	0.7	1.12	2.06	−1.15	2.78	1.71	1.49	0.06	0.7
2D	CH	TCU075	1.5	0.88	5.24	0.98	1.21	1.32	2.18	0.08	0.68
2D	IV79	EC Array #10 (FP)	8.6	0.41	2	0.44	3.12	1.55	2.28	0.04	0.57
2D	NP	N Palm Springs	8.2	0.73	1.37	−0.6	5.00	1.66	2.7	0.08	0.69
2D	CL	Gilroy Array #6	3.1	0.49	0.88	−0.47	6.10	1.46	2.72	0.07	0.83
2D	IR	Sturno	32	0.36	1.66	−0.33	3.12	1.71	2.89	0.21	0.37
3A	LP	Saratoga W Val (FP)	14	0.62	4.01	0.43	1.27	1.9	0.03	0.46	0.59
3A	IV79	EC Array #3	9.3	0.40	4.44	−0.31	1.36	1.82	0.2	0.1	0.72
3A	CH	TCU068	1.1	1.77	6.05	1.49	0.56	1.85	0.26	0.29	0.75
3A	IV79	Holtville PO	7.5	0.49	4.22	0.42	1.44	1.78	2.95	0.12	0.78
3A	IV79	EC Meloland	0.5	0.91	2.52	0.79	2.26	1.92	0.27	0.08	0.78
3B	IV79	EC Array #7	0.6	1.09	3.75	0.76	1.74	2.13	0.73	0.18	0.81
3B	CM	Cape Mendocino (FP)	8.5	1.25	3.44	−0.46	1.41	1.79	0.85	0.51	0.61
3B	IR	Sturno (FP)	10.8	0.52	3.13	−0.55	1.95	2.02	1.11	0.14	0.77

Table 3 continued

Bin[a]	ID	Station (component)	D [km]	|PGV| [m/s]	T_p [s]	A [m/s]	ω [rad]	γ	Φ	E_p	E_{th}
3C	CH	TCU103	6.1	0.62	8.9	−0.55	0.82	2.13	1.49	0.24	0.73
3C	IV79	EC Array #6	1.0	1.10	3.63	0.97	1.68	2.03	1.5	0.04	0.92
3C	LP	Gilroy Historic Bldg.	13	0.42	1.17	0.35	4.22	2.09	1.62	0.13	0.71
3C	IV79	EC Array #8	3.8	0.49	3.99	0.42	1.41	2.05	1.87	0.22	0.73
3D	CH	TCU102	1.8	1.13	3.84	−0.57	0.79	2.23	2.08	0.73	0.53
3D	IV79	EC Array #4	4.2	0.77	4.32	0.74	1.48	1.9	2.14	0.07	0.87
3D	IV79	EC Array #5	1.0	0.91	3.36	0.88	1.67	1.86	2.28	0.07	0.83
3D	CH	TCU101	2.9	0.68	5.54	−0.44	0.72	2.15	2.29	0.31	0.7
3D	LP	LGPC	6.1	1.09	4.28	−0.87	1.62	2.08	2.53	0.59	0.54
4A	TA	Tabas	2	1.21	5.28	−0.98	1.18	2.55	0.15	0.22	0.71
4B	BU	Bucharest (NS)	115	0.74	1.88	−0.62	3.09	2.34	0.5	0.05	0.86
4C	MH	Coyote Lake Dam (FP)	0.1	0.80	0.72	0.68	7.49	2.66	1.21	0.13	0.78
5D	NO	Jensen Filter Plant	6.2	0.76	2.72	−0.52	2.25	3.77	2.06	0.35	0.71

[a] Bin numbers 1, 2, 3, 4 and 5 correspond to γ value ranges of [0.75–1.25], [1.25–1.75], [1.75–2.25], [2.25–2.75], [2.75-4], respectively. Bin letters A, B, C, D and E correspond to ϕ value ranges of $[-\pi/8 - \pi/8]$, $[\pi/8 - 3\pi/8]$, $[3\pi/8 - 5\pi/8]$, $[5\pi/8 - 7\pi/8]$, respectively

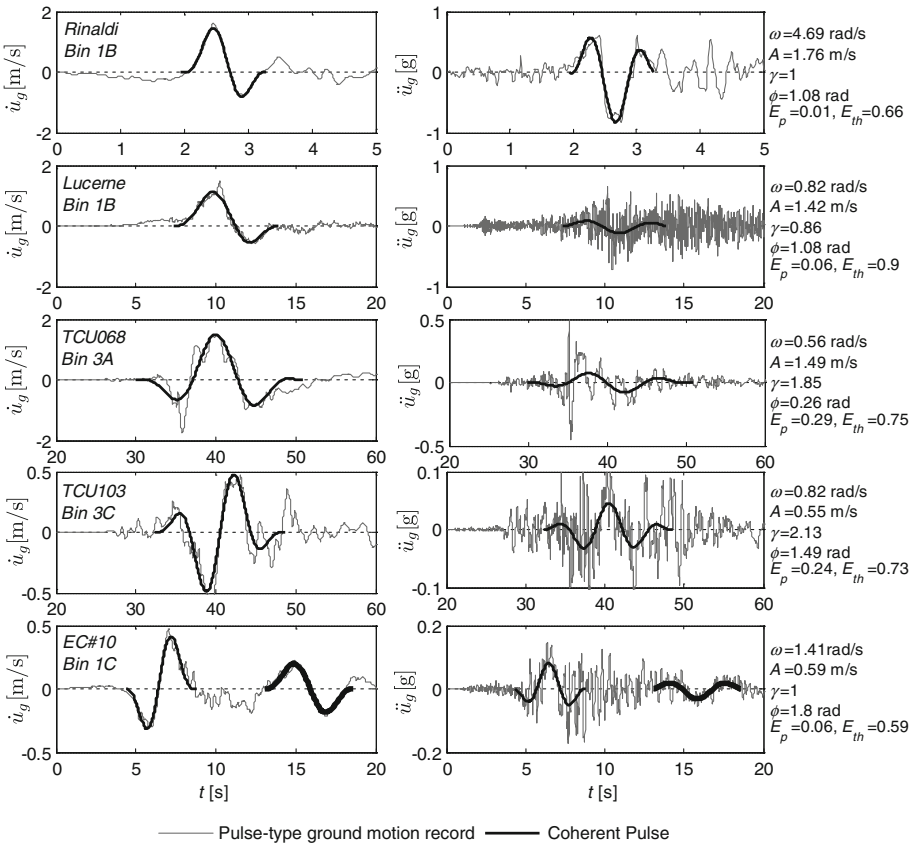

Fig. 4 Velocity (*left column*) and acceleration (*right column*) time histories of five pulse-type earthquake records with fitted M&P wavelets and associated pulse parameters. Refer to Sect. 3.2.2 for definition of pulse parameters and Table 3 for bin definitions. In the bottom row, the pulse parameters are given for the initial pulse

estimates for the parameters involved and the time period over which the optimization is carried out. The following procedure was used to minimize the subjectivity related to picking initial values. The parameter A was estimated as the PGV, ω was estimated as $2\pi / T_p$ and the parameters γ and ϕ were determined by inspection. The optimization window was defined as the broad time interval including all half-cycles. A single iteration of the fitting procedure was conducted to obtain first estimates for the next round of iteration where the pulse window is defined according to Eq. 3. Iterations were repeated until convergence was observed. The procedure was observed to be stable; reasonable changes in the initial estimates of γ, ϕ, or the optimization time window did not influence the final results.

Figure 4 presents the velocity and acceleration time histories of some records with the fitted velocity pulse and its derivative, the coherent acceleration pulse. The M&P wavelet effectively represents records with different periods, amplitudes and shapes. For example, the Rinaldi record (Fig. 4, top row) features a forward directivity pulse with a much smaller period and a larger amplitude than the Lucerne pulse (Fig. 4, 2nd row). The velocity pulses of these records, which are similar in shape, are captured effectively in both cases. Note that the coherent acceleration pulse is clearly visible in the Rinaldi record, but it is masked

by high amplitude and high frequency data in the Lucerne record. Two near-field records from the Chi-Chi earthquake (Fig. 4, 3rd and 4th rows) display forward directivity pulses, although with considerably different pulse shapes. The TCU068 velocity pulse is similar to an asymmetric cosine pulse and has fewer significant half cycles than the TCU103 pulse. The fitted pulse parameters reflect this qualitative observation.

More significantly, comparison of the Chi-Chi records to the Rinaldi record demonstrates that the quality of fit is not consistent. While the M&P wavelet captures the coherent velocity pulse of both Chi-Chi records, the velocity record is contaminated by other pulses. In the case of TCU068, an acceleration pulse with a relatively low frequency and high amplitude has a noticeable trace in the first pulse cycle. For TCU103, several relatively high amplitude acceleration pulses mask the coherent velocity pulse. These high amplitude or low frequency acceleration pulses can affect rocking response. To account for their presence, a quality of fit of expression is proposed:

$$E_p = \frac{\int_{t_{p0}}^{t_{pf}} \dot{u}_r^2 dt}{\int_{t_{p0}}^{t_{pf}} \dot{u}_g^2 dt} \tag{4}$$

where $t_{p0} = t_0 - \frac{\pi\gamma}{\omega}$ and $t_{pf} = t_0 + \frac{\pi\gamma}{\omega}$ are fitted M&P wavelet initiation and termination times, and $\dot{u}_r = \dot{u}_g - \dot{u}_p$ is the residual velocity record after the pulse has been subtracted from the original velocity record. The value of E_p lies between zero and one, and a low E_p suggests a good quality pulse fit.

Figure 4 (5th row) also shows the necessity of defining a quality of fit parameter which describes the dominance of a fitted velocity pulse over the whole time history. The EC Array #10 velocity record features two coherent velocity pulses. Additionally, a descriptor is necessary to discriminate records which have a higher frequency velocity pulse which does not dominate the record. The following is proposed as an indicator of the dominance of the velocity pulse over the entire time history:

$$E_{th} = \frac{\int_{-\infty}^{+\infty} \dot{u}_p^2 dt}{\int_{-\infty}^{+\infty} \dot{u}_g^2 dt} \tag{5}$$

A high E_{th} suggests that the velocity pulse effectively dominates the time history. The pulse parameters and the associated quality of fit parameters (Eqs. 4, 5) are also presented in Table 3.

3.2.3 Binning of records

Previous studies have defined empirical attenuation relationships which correlate seismological parameters such as moment magnitude M_w, distance to causative fault D and local geology to the intensity measures PGV and T_p for near-field records with forward directivity pulses (e.g. Bray and Rodriguez-Marek 2004). For the records in Table 3 which have a good quality of fit (defined by $E_p < 0.15$ and $E_{th} > 0.6$), least squares regression analyses with an intercept fixed at the origin are carried out between between PGV and T_p and the fitted pulse parameters A and ω, respectively (see Fig. 5). These results indicate an almost one to one linear correlation. A clear correlation still exists when all of the ground motions in Table 3 are considered, although the best-fit regression line becomes $A = 0.87$ PGV, suggesting that PGV slightly overestimates A for lower quality pulse fits (not shown). These results suggest that if local geology and possible fault mechanisms are known, the values of A and ω can be estimated with the values of PGV and T_p. However, there are no attenuation relationships available for predicting γ and ϕ which define the pulse shape. Bray and Rodriguez-Marek

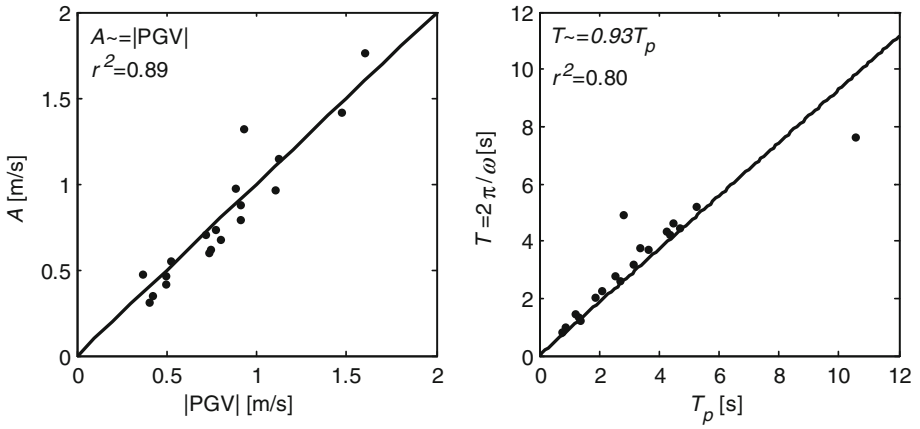

Fig. 5 The relationship between the fitted pulse intensity parameters A and ω and the ground motion IMs PGV and T_p, respectively

(2004) suggest that for earthquakes with non-uniform slip, γ depends on 'the instrument distance relative to the asperities' and therefore is 'difficult to estimate a priori'.

In this study, to investigate the rocking response to earthquake records systematically, the pulse-type earthquakes listed in Table 3 have been categorized according to their pulse shapes, arranging them into a discrete number of bins. Each record was assigned a bin, identified by a number (defining the γ range of the bin) followed by a letter (describing the ϕ range of the bin), such as 1B. In Table 3, a legend specifies the range of γ and ϕ of each bin and in Fig. 4 some records representative of their 'bins' can be observed.

3.3 Role of pulses in the response to pulse-type earthquakes

In this section, the ability of fitted pulses alone to describe the rocking response to pulse-type earthquakes will be further investigated. To do this, the physical similarity of the rocking response to M&P wavelets will be utilized.

3.3.1 Physical similarity of the response to M&P wavelets

An earlier study by the authors shows that the response of flexible rocking structures to trigonometric pulses is physically similar (Acikgoz and DeJong 2012). This scaling property allowed the representation of results in a concise manner for a range of different structures. Here, the property of physical similarity will be used to evaluate the response to M&P wavelets using Buckingham's π-theorem. Assuming that the structure is excited horizontally by an M&P wavelet, the response parameter of interest is expressed in terms of the input parameters as follows:

$$\theta = f(\omega_n, \zeta, \alpha, p, g, \omega, A, \gamma, \phi, t) \tag{6}$$

There are ten input parameters and each of these parameters can be described by two fundamental dimensions: length [L] and time [T]. Therefore eight input parameters are required to describe the dimensionless rocking amplitude:

$$\frac{\theta}{\alpha} = f\left(\frac{\omega_n}{p}, \zeta, \alpha, \frac{\omega}{p}, \frac{Ap}{g\tan\alpha}, \gamma, \phi, \tau\right) \tag{7}$$

where $\tau = pt$ describes the dimensionless time. The dimensionless frequency (ω/p) and strength of excitation ($Ap/(g\tan\alpha)$) together determine the intensity of the pulse, while γ and ϕ control the pulse shape. It is important to note that the dimensionless strength of excitation term is independent of the frequency of excitation, allowing an intuitive definition of the range of realistic strength of excitation values depending on values of A, p and α (see Sect. 4.1.1). Furthermore the multiplication of the dimensionless terms (ω/p) and ($Ap/(g\tan\alpha)$) results in the dimensionless term ($A\omega/(g\tan\alpha)$) which provides an intuitive but approximate description of the acceleration amplitude of the pulse and its relation to the rigid body uplift threshold. Numerical simulations confirm that the system is physically similar when excited with the M&P wavelet (not shown). Therefore, two structures which have different non-dimensional groups (e.g., different ω, A and R_0) but identical dimensionless groups (e.g. identical ω/p, $Ap/(g\tan\alpha)$, γ, ϕ), will have the same dimensionless response.

3.3.2 Physical similarity of the response to pulse-type earthquakes

For large structures which are less sensitive to high frequency elements of ground motion, long duration pulses may govern the response as indicated in Fig. 2. To further test this hypothesis, the time history response of a specific structure to a ground motion and its fitted pulse can be directly compared (e.g. DeJong 2012). However, the ground motion records listed in Table 3 have significantly different characteristics. Comparing the responses of these records and the fitted pulses for an arbitrary structure might not yield systematic results.

The results of the dimensional analysis performed in the previous section suggest that different structures subjected to M&P wavelets with different dimensional groups, will have identical response if the dimensionless groups are the same. Using this result, the pulse-type earthquakes can be treated as if they are M&P wavelets with fixed frequency, amplitude and shape. It is possible then to arrange the structural size and scale the amplitude of the ground motion to achieve target intensity parameters (ω/p and $Ap/(g\tan\alpha)$).

Figure 6 illustrates the dimensional response of two different structures subjected to the amplitude scaled EC Diff Array record and an M&P wavelet. The velocity pulse of the record and the wavelet have different frequency and amplitude, however their pulse shapes are governed by the same γ and ϕ parameters. The chosen structures have the same slenderness and damping, but the structure utilized in the investigation of the record is almost nine times larger and three times more flexible. Therefore it is not surprising that the dimensional rocking response to these ground motions is quite different (Fig. 6, top row). However, when the response and input parameters are non-dimensionalized, good agreement is observed (Fig. 6, bottom). This agreement is better during the dimensionless time period where the pulse is observed. The good correlation of the results indicates that the velocity pulse governs the response.

Figure 6 only exemplifies behavior for a single structure and a single set of ground motion intensity parameters. More generally, the spectral rocking response to the amplitude scaled EC Diff Array record and a fitted M&P wavelet with similar dimensionless parameters is presented in Fig. 7. A range of target dimensionless ground motion intensities ($\omega/p = 3, 4, 5, 6$ and $Ap/(g\tan\alpha) = 0.3, 0.5, 0.7, 0.9$) were specified and ground motion amplitude was scaled accordingly. Appropriate pulse parameters and structural sizes were picked for the M&P wavelet with the same shape (γ and ϕ) as the record's velocity pulse. To ensure that only large structures are considered, an upper limit of $p = 1$ was specified. Unrealistically large structures and scaling factors were occasionally required to achieve target intensity parameters, however, this was not considered an issue for evaluating the ability of wavelets to capture dimensionless response. Figure 7 shows that the velocity pulses adequately describe

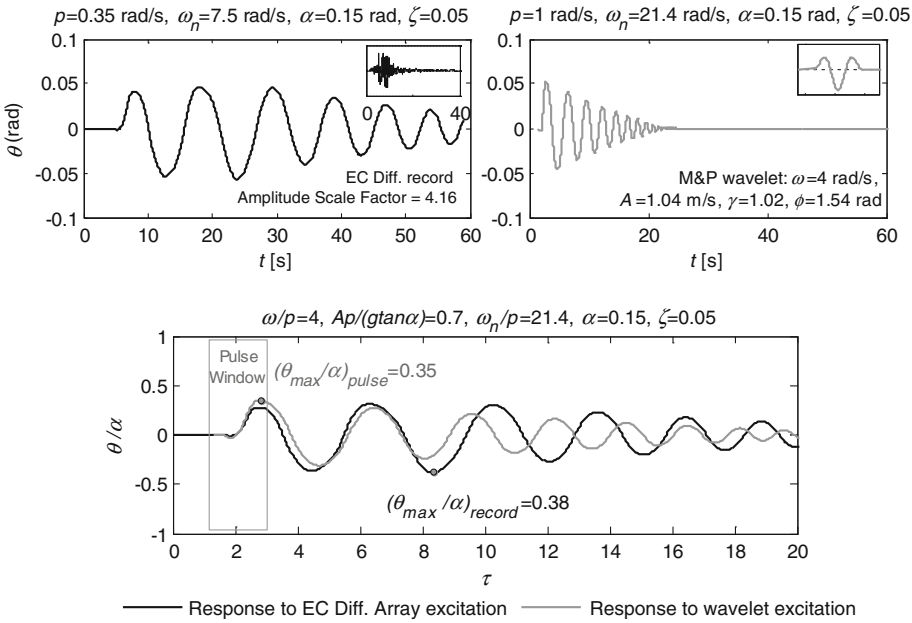

Fig. 6 The dimensional rocking response of two different structures to the scaled EC Diff Array record (*top left*) and an M&P wavelet (*top right*) and the similar dimensionless representation of both responses (*bottom*)

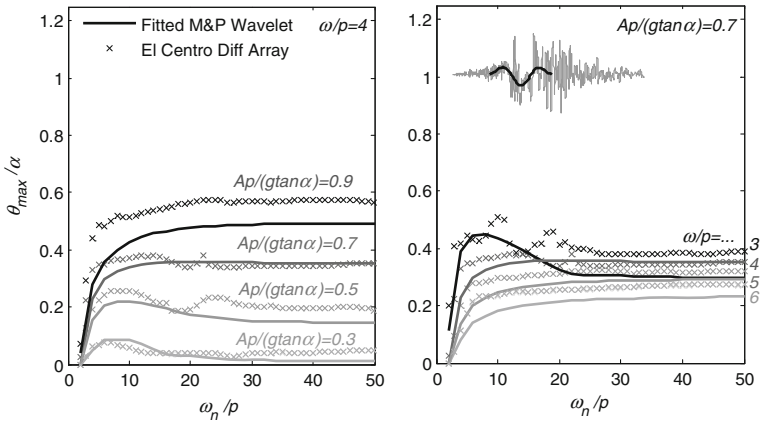

Fig. 7 Dimensionless rocking spectra for the scaled EC Diff Array record and its fitted wavelet for different pulse amplitudes (*left*) and frequencies (*right*). The acceleration record (*solid grey line*) and the fitted wavelet (*solid black line*) are also shown inset

the response over a range of intensities for structures with different flexibility/scale. For this record, which has a good quality of fit ($E_p = 0.12$ and $E_{th} = 0.72$), the error in response estimations with wavelets does not exceed 0.1α.

If velocity pulses dominate, earthquake records with similar pulses should cause similar dimensionless response. Using the ground motion bins specified in Sect. 3.2.3, the records in each bin which satisfy certain quality of fit criteria ($E_p < 0.15$ and $E_{th} > 0.6$) were scaled to a specified earthquake intensity, and appropriate structural sizes were chosen. The ground motion bin is represented by a pulse which has the mean γ and ϕ of the bin. In

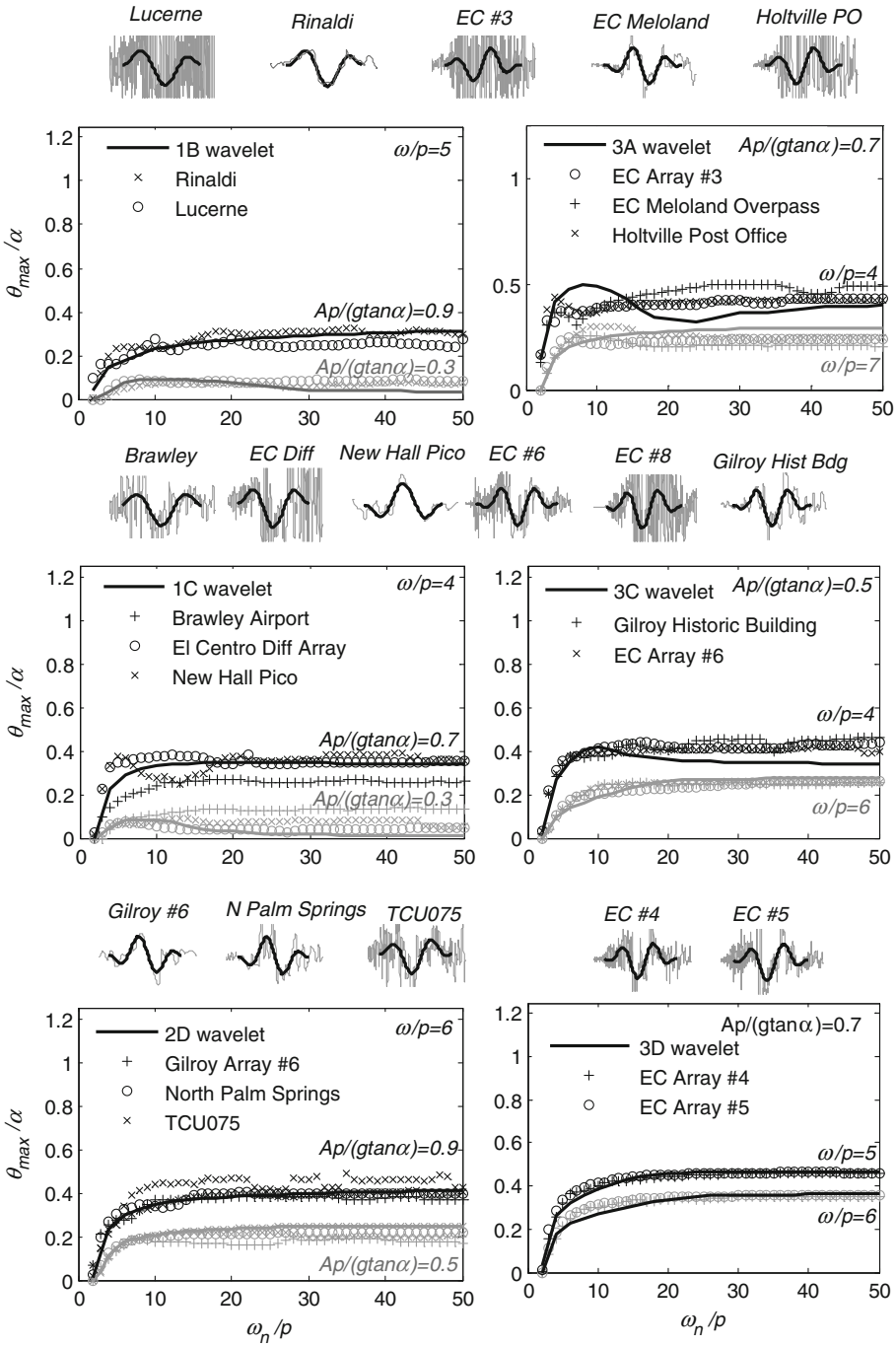

Fig. 8 Dimensionless rocking spectra for records from six different ground motion bins (1B, 1C, 2D, 3A, 3C, 3D) and for corresponding representative bin wavelets with varying intensity. The acceleration trace (*grey solid line*) and the fitted wavelets (*black solid line*) for each ground motion record are shown between the rocking spectra plots

Fig. 8, the results for 6 different ground motion bins are presented. For instance, the Lucerne and Rinaldi records of bin 1B were scaled to have the ground motion intensity $\omega/p = 5$ and $Ap/(g\tan\alpha) = 0.3, 0.9$ in Fig. 8 (top left). The rocking response to an M&P wavelet (representative of bin 1B) with $\gamma = 1.0$ and $\phi = \pi/4$ rad and similar dimensionless intensities is also presented for reference.

Figure 8 confirms that velocity pulses can single-handedly describe the response for numerous records with different target intensities. This finding indicates that the emergent portion of the time history, prior to the initiation of the pulse, was generally insignificant. Prior high frequency oscillations might have caused uplift, but did not sustain rocking motion. Therefore rocking amplitude at the initiation of the coherent pulse was negligible. While differences in uplift location might have been facilitated by high frequency acceleration pulses on the velocity pulse, the response seems to be insensitive to these small changes for $\omega/p \geq 4$.

3.3.3 Limitations of pulse based analysis

There are certain cases where the description of pulse-type earthquakes with M&P wavelets may be inadequate. For example, when the dimensionless frequency is small ($\omega/p < 4$), the rocking response is sensitive. In this region, not only can small changes in ground motion intensity cause large differences in rocking amplitude, but high frequency acceleration pulses can also affect the response by facilitating earlier uplift or modifying the amplification mechanisms. Figure 9 (top row) illustrates two response comparisons from this region. For the lower amplitude case ($Ap/(g\tan\alpha) = 0.3$), the 3B wavelet underestimates the rocking amplitude of stiff structures ($\omega_n/p > 6$) significantly, as it does not predict uplift. Contrastingly, the 3B wavelet overestimates the rocking amplitude for $Ap/(g\tan\alpha) = 0.9$. Although the predictions are poor in this case, better response fits can also be obtained in this region (see Figs. 7, 9 (top right)).

Another important consideration is the emergent portion of the time histories. As expressed earlier, it is unlikely for forward directivity records to have low frequency components preceding the coherent velocity pulse. This ensures that at the initiation of the coherent pulse, rocking motion is negligible. However, in the Parachute Test Site record, a low frequency acceleration pulse precedes the coherent pulse (see Fig. 9, middle left). This acceleration pulse introduces significant rocking amplitude at the initiation of the coherent pulse, changing the amplification mechanisms entirely. As can be observed from the two response fits with M&P wavelets, the response may be overestimated or underestimated depending on pulse intensity. It should be noted that the time history dominance parameter E_{th} does not capture the critical presence of this acceleration pulse.

The response fits in Fig. 8 were only for records which had quality of fit parameters within the range $E_p < 0.15$ and $E_{th} > 0.6$. This implied that the M&P wavelets described the coherent pulse which dominated over the time history reasonably well. However, as demonstrated earlier in Fig. 4, relatively large acceleration pulses may distort the velocity record or the coherent pulse may not dominate the time history. As an example of how large acceleration pulses affect the response, the response to Cape Mendocino record ($E_p = 0.51$) is shown in Fig. 9 (middle right). It can be seen that the presence of a large acceleration pulse decreases the response in the two cases investigated. In the last row of Fig. 9, two records are presented which have $E_{th} < 0.6$. The Sturno record ($E_{th} = 0.35$) has two long and coherent pulses, and demonstrates that analyses based on a single pulse may be inadequate when multiple coherent pulses are observed. The Pacoima Dam record ($E_{th} = 0.5$) has a single coherent pulse with a relatively high frequency, and shows that the pulse provides

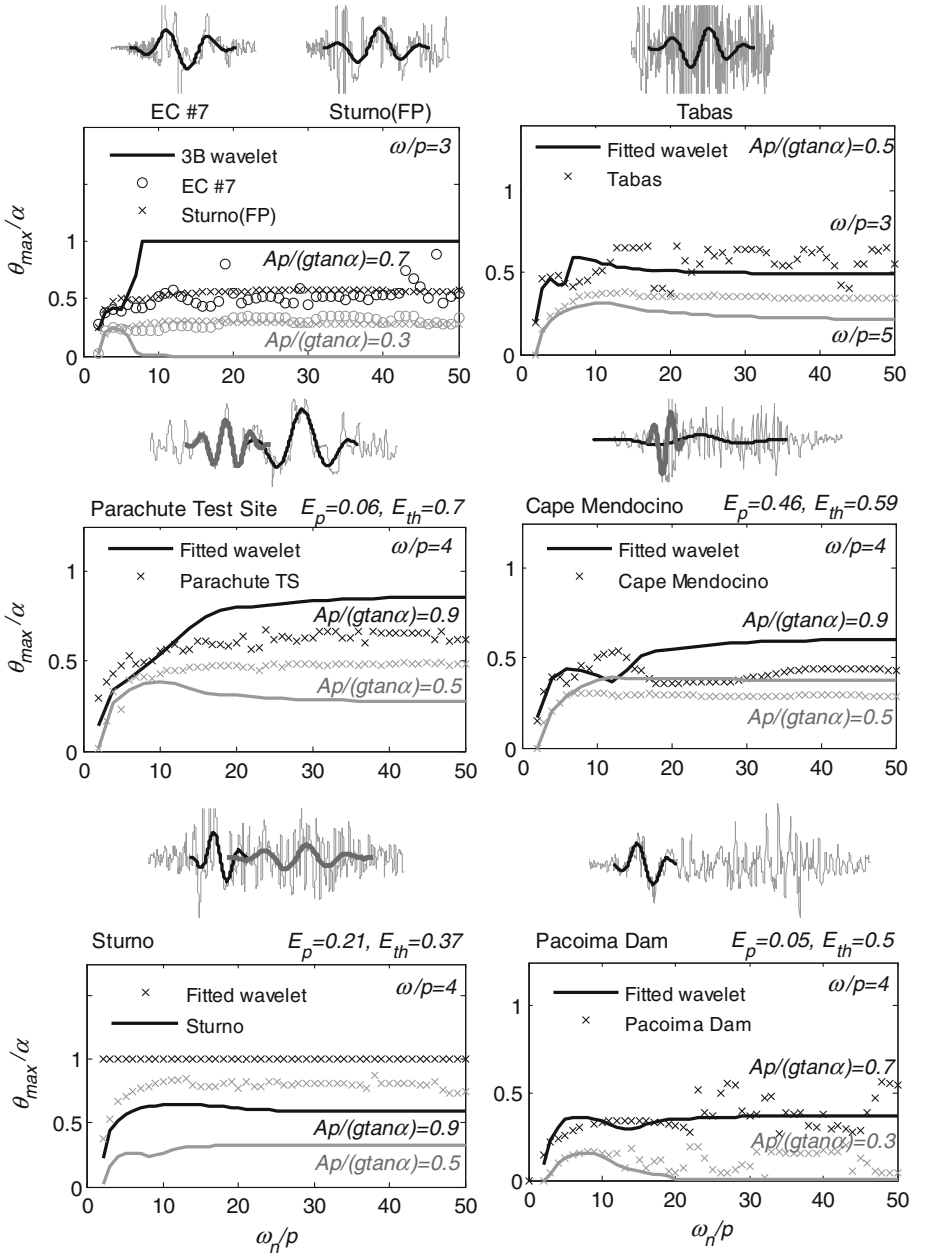

Fig. 9 Dimensionless rocking spectra for various specific records (with varying scaled amplitudes) and their corresponding fitted wavelets. The acceleration traces (*grey solid lines*) with both fitted wavelets for the coherent velocity pulse (*black solid lines*) and other highlighted pulses (*thick grey lines*) are also shown in between the rocking spectra plots

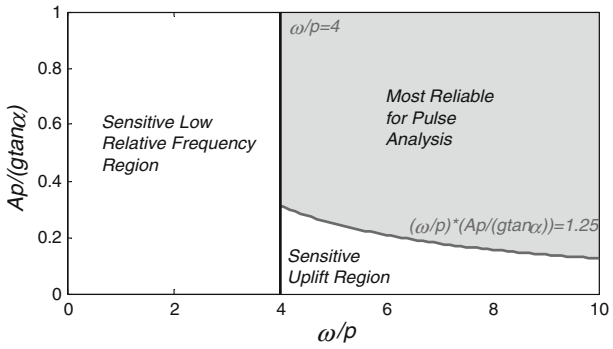

Fig. 10 Map highlighting dimensionless intensity regions where pulse analysis is more reliable and where it is more sensitive

a good average estimate of the response though it cannot capture the interaction of pulses which affects the response randomly (DeJong 2012).

In summary, pulse based analysis might be inaccurate due to: (i) the increased sensitivity of rocking motion at low relative frequencies, (ii) initial rocking caused by emergent time histories, (iii) low frequency acceleration pulses and (iv) lack of coherent pulse dominance over the time history. Based on the previous discussion, a map is proposed which highlights the intensity regions where rocking motion is sensitive and where pulse analysis is most reliable (see Fig. 10). Furthermore, a sensitive uplift region is specified below the curve $A\omega/(g\tan\alpha) = 1.25$ where pulses might not predict uplift although higher frequency elements of the ground motion might facilitate it. These regions were defined conservatively based on the analyses presented in Figs. 7, 8 and 9 and are useful for interpreting the demand maps which follow in Sect. 4.

4 Predicting the rocking response

In Sect. 3, it was shown that fitted velocity wavelets can effectively replace pulse-type records to estimate maximum rocking amplitude. This result could be particularly useful in predicting maximum rocking response. However, a better understanding of how pulse parameters affect the maximum rocking response is required.

4.1 Parametric analysis of pulse parameters

4.1.1 Effect of pulse intensity parameters

The velocity pulse intensity parameters A and ω vary significantly depending on the magnitude of the earthquake, distance to the source, orientation of the site, etc. Mavroeidis and Papageorgiou (2003) have described A as a stable parameter which typically does not exceed 1.3 m/s. Therefore a conservative theoretical upper bound of 1.5 m/s was defined for A (only a few records' amplitude exceed this value, see Mavroeidis and Papageorgiou 2003 for a detailed discussion). Only ground motions with PGV higher than 0.3 m/s were considered in this study. No lower and upper bound value was specified for the velocity pulse frequency, however the ground motion records used in this study suggest a typical range of 0.75–6.0 rad/s (see Fig. 5).

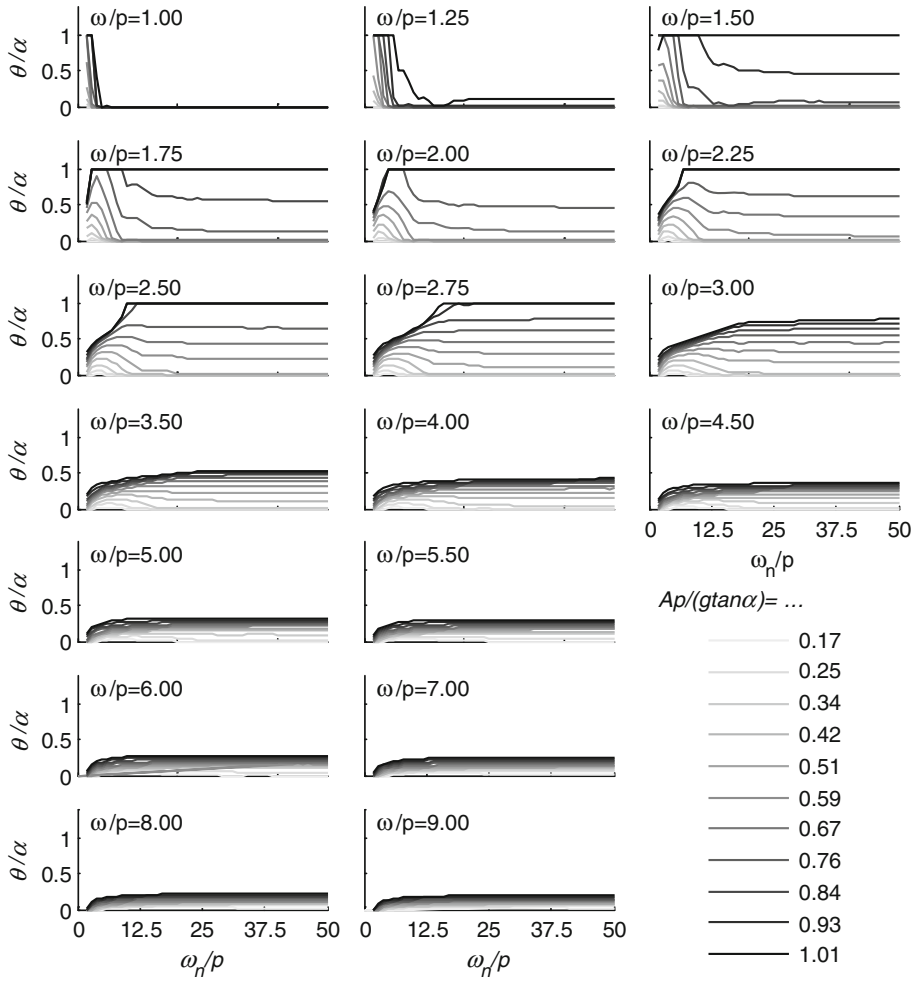

Fig. 11 Dimensionless rocking spectra for M&P wavelets with a range of dimensionless frequencies and amplitudes but the same pulse shape

Figure 11 shows rocking spectra for a structure subjected to a range of different intensity velocity pulses which have a shape similar to a cosine pulse (Bin 1A: $\gamma = 1, \phi = 0$). Each subfigure shows the rocking spectra of the structure under the influence of a dimensionless frequency of ω/p and a range of dimensionless amplitudes $Ap/(g \tan\alpha)$. The dimensionless parameters utilized here represent the whole range of permissible pulse-type excitations for large structures where $p \leq 1$ and $\alpha \geq 0.15$.

In Fig. 11, results for the dimensionless frequency range of $1.5 < \omega/p < 3$ further demonstrate that low frequency excitations are detrimental to rocking structures. Interestingly, in the lowest frequency range of $\omega/p < 1.5$, high rocking amplification and overturning is only observed for more flexible structures. For stiffer structures, these excitations do not cause uplift and therefore, even for the highest amplitude cases, no rocking is observed. Further-

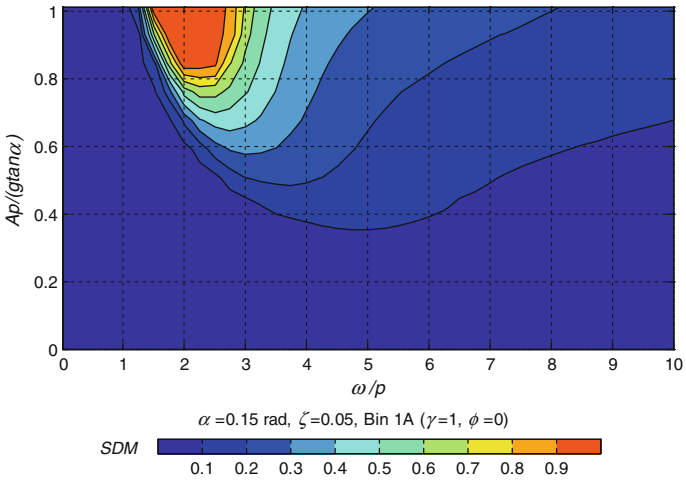

Fig. 12 Dimensionless spectral demand map for a specified pulse shape (Bin 1A)

more, the amplification of rocking due to increased flexibility is evident in all spectra where $\omega/p < 3$. However, for $\omega/p > 3$, increased flexibility generally results in reduced rocking. This observation agrees with the trends observed in a previous study investigating how overturning behavior is affected by increasing flexibility (Acikgoz and DeJong 2012). Also note that the shape of the response spectrum changes significantly for $\omega/p < 3$ and is sensitive to the amplitude and frequency parameters. However, outside this range the response is less sensitive.

While the information presented in Fig. 11 is dimensionless and therefore addresses many different structures, the variations in the response spectrum do not allow an understanding of the destructiveness of the pulse, which can be better evaluated using the spectral demand measure introduced in Sect. 3.1.2. The dimensionless spectral demand map presented in Fig. 12 condenses the data in Fig. 11 to a single contour map which conveys the general destructiveness of an earthquake, at the cost of presenting structure specific response. In particular, note that the spectral demand measure underestimates the effect of flexibility on the response and should therefore not be used in analysis and design of a specific structure, but rather as a means to compare different regions of intensity for a broad range of flexibilities. In the next section, similar maps are used to discuss the effect of pulse shape parameters on rocking response.

4.1.2 Effect of pulse shape parameters

While the effect of pulse shape has been observed to be insignificant for various structures fixed to the ground (Mavroeidis et al. 2004; Sehhati 2008), their effect on rocking structures may be significant. It is particularly important to understand how these parameters affect rocking response as it is difficult to estimate these parameters a priori (see Sect. 3.3.2).

The parameter γ controls the number of half cycles of a given pulse. In Fig. 13, the rocking spectra for two different intensities are presented for $\gamma = 1, 1.5, 2$ and 2.5, while $\phi = 0$, yielding an asymmetric velocity pulse. The bin numbers of these wavelets are also shown. Alongside the rocking spectra, the dimensionless spectral demand maps for the same bins are presented. The spectral demand maps show that increasing γ generally increases rocking

response. This is particularly evident in the low relative frequency range ($\omega/p < 4$) due to the lengthening of the envelope function of the M&P wavelet, which effectively emphasizes the higher amplitude regions of the underlying harmonic. However, as the rocking spectra show, this effect cannot be generalized to all intensities and natural frequencies. At certain values of intensity and flexibility, lower γ values result in higher rocking amplitudes. In addition, an increase in γ reduces the smoothness of the SDM, indicating less consistent behavior. This is due to the variable effect of increasing the number of half-cycles, effectively causing the interaction of multiple pulses.

Similarly, the effect of ϕ is investigated in Fig. 14, where a constant value of $\gamma = 1$ is specified. Bins 1A, 1B, 1C and 1D were considered. The spectral demand maps show that generally the asymmetric velocity pulse ($\phi = 0$ rad) causes much higher rocking than the symmetric pulse ($\phi = \pi/2$ rad). This result is in agreement with previous investigations which showed sine acceleration pulses to be much more destructive than cosine acceleration pulses (e.g. Zhang and Makris 2001). However, as with γ, this trend is not uniformly true. At certain intensities and natural frequencies, symmetric pulses caused a larger response, as demonstrated by the rocking spectra in Fig. 14. In general, Figs. 13 and 14 identify certain behavioral trends, but also indicate that a single pulse shape cannot be specified as the worst-case pulse. It is therefore important to quantify how much difference is observed between the responses of ground motion bins.

4.1.3 Median, maximum and dispersion of response to ground motion bins

In the previous sections, the SDM was used to evaluate the effect of pulse intensity and shape parameters on the response in a qualitative manner. To quantify the differences between the responses to different ground motion bins, it is more accurate to evaluate maximum rocking amplitude. Therefore, the maximum rocking amplitude (θ_{max}/α) will instead be presented on dimensionless demand maps for discrete values of relative stiffness (ω_n/p).

Figure 15 presents two dimensionless contour maps for each specified value of ω_n/p. The left column shows the median of the maximum rocking amplitude, amongst the 20 bins defined in Table 3, and the right column shows the maximum response of any bin. To cover a range of relative stiffnesses, results are presented for $\omega_n/p = 4$, 10 and 24. The 4th row represents the results for a rigid structure, computed using the classical rigid rocking equations of motion (Housner 1963). This serves as a benchmark for the other results.

For $\omega_n/p = 4$, the maximum demand maps are notably conservative compared to the median demand maps. In particular, in the sensitive rocking region of $\omega/p < 4$, high rocking contour lines ($\theta_{max}/\alpha \geq 0.9$) penetrate into lower relative frequency and dimensionless amplitude regions. This shows that certain ground motion bins cause significantly more rocking motion than others. These results also hold for $\omega_n/p = 10$, 24 and the rigid case. As the relative stiffness increases, the variability of the response is significant over a wider range of dimensionless frequencies and amplitudes. Note that the last two rows of Fig. 15 are nearly identical.

The median absolute deviation of the maximum rocking amplitude resulting from all ground motion bins is plotted in Fig. 16 for relatively flexible $\omega_n/p = 4$, and relatively stiff ($\omega_n/p = 24$) structures. The median absolute deviation in the sensitive rocking region reaches 0.4α and may be as high as 0.15α in less sensitive regions. This result shows that the possible effect of different pulse shapes should be considered in the analysis and design of rocking structures to achieve a better estimate of maximum rocking under the influence of pulse-type earthquakes. However, for preliminary design or assessment, the median or maximum value of all bins could be used to estimate expected rocking.

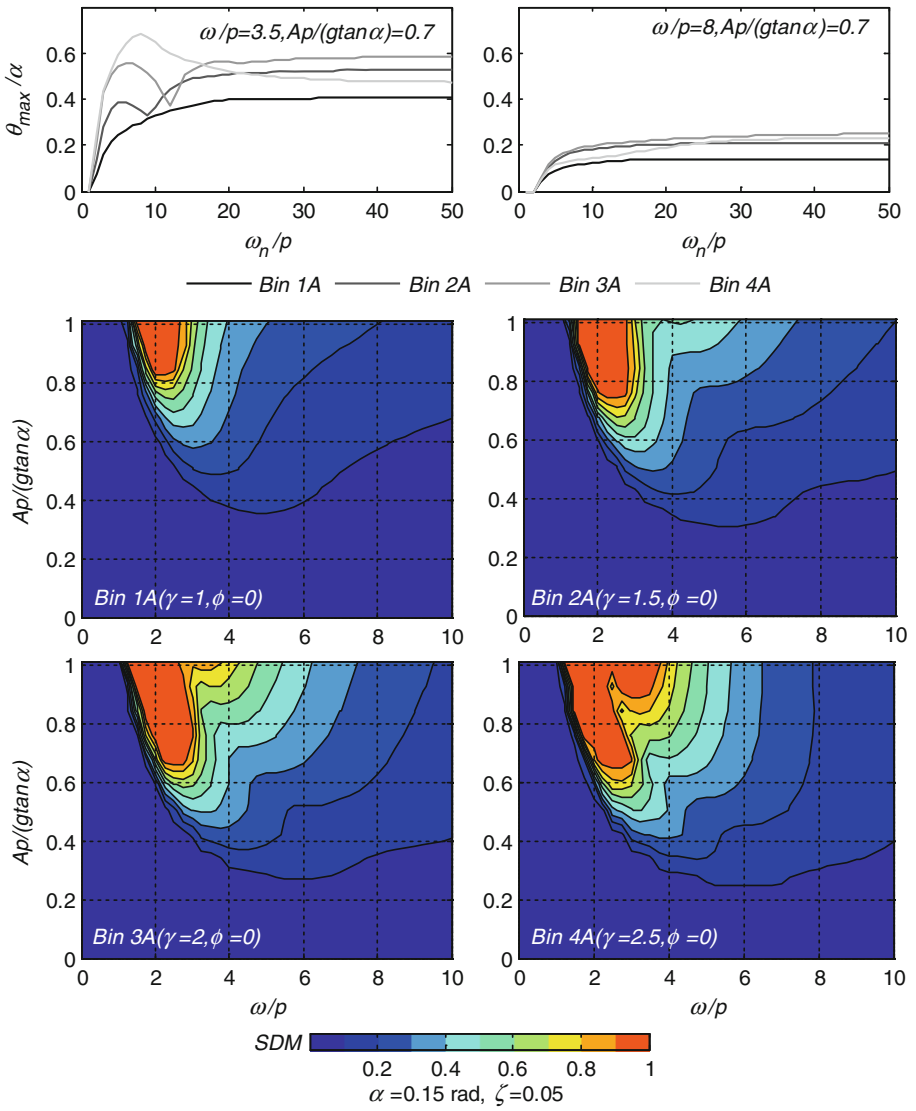

Fig. 13 The effect of γ on maximum rocking demand: dimensionless rocking spectra for wavelets with given intensities but changing γ (*top row*), and dimensionless spectral demand maps for wavelets representing four different bins

4.2 Prediction of maximum rocking response

In this section, a probabilistic approach is proposed to predict the maximum rocking response to pulse-type records. Prediction of the response to non-pulse type records is briefly discussed.

4.2.1 Pulse-type records

The initial aim is to estimate the probability that the maximum rocking will exceed a design value provided that: (i) a pulse is known to occur and (ii) the period and amplitude of the

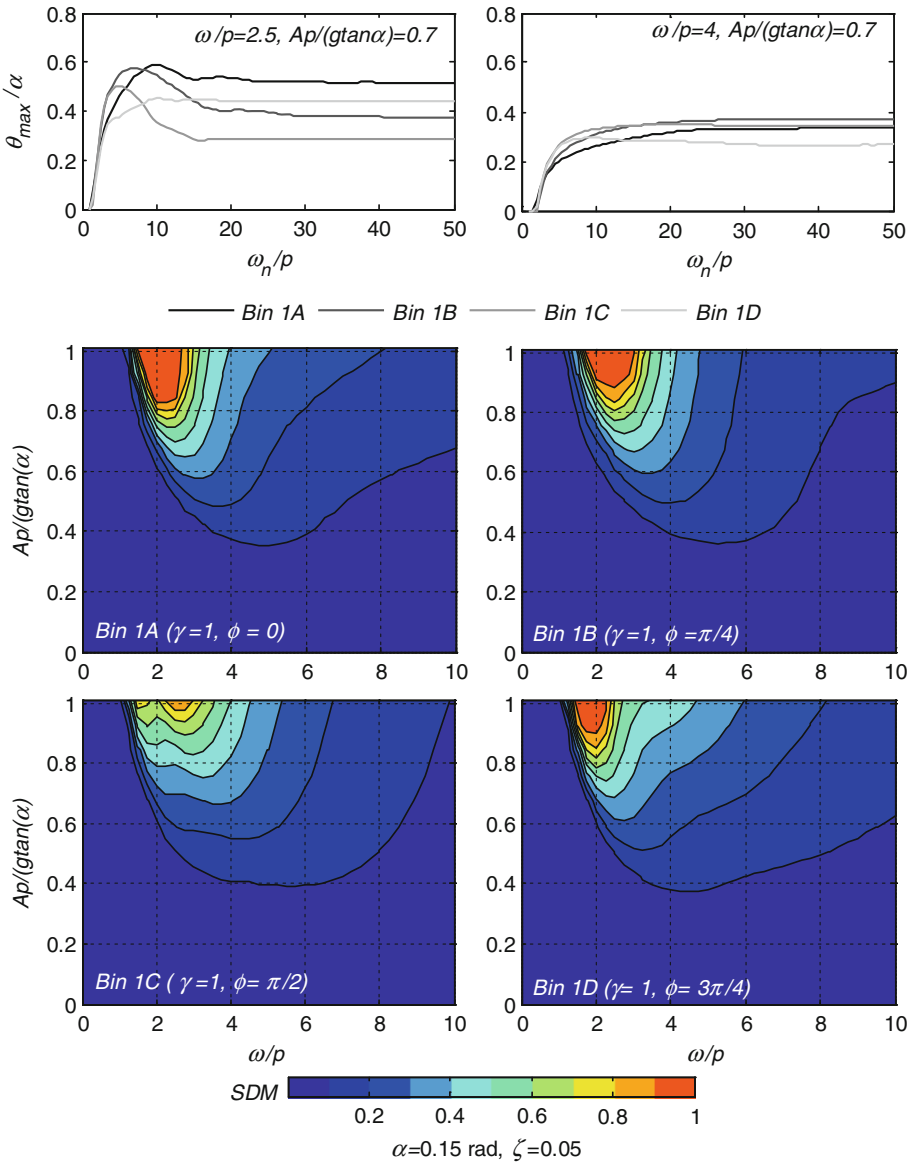

Fig. 14 The effect of ϕ on maximum rocking demand: dimensionless rocking spectra for M&P wavelets with given intensities but changing ϕ (*top row*), and dimensionless spectral demand maps for wavelets representing four different bins

pulse are known for the given scenario. Therefore the objective is to evaluate the following expression:

$$\lambda_{scenario,pulse}(x) = P\left((\theta_{\max}/\alpha)_{scenario,pulse} > x|A,\omega\right) \tag{8}$$

where the notation P(Y|Z) is the probability density of Y conditioned on knowledge of Z and $\lambda_{scenario,pulse}$ represents the cumulative probability density function of exceedance of the maximum rocking amplitude x for a pulse-type earthquake scenario.

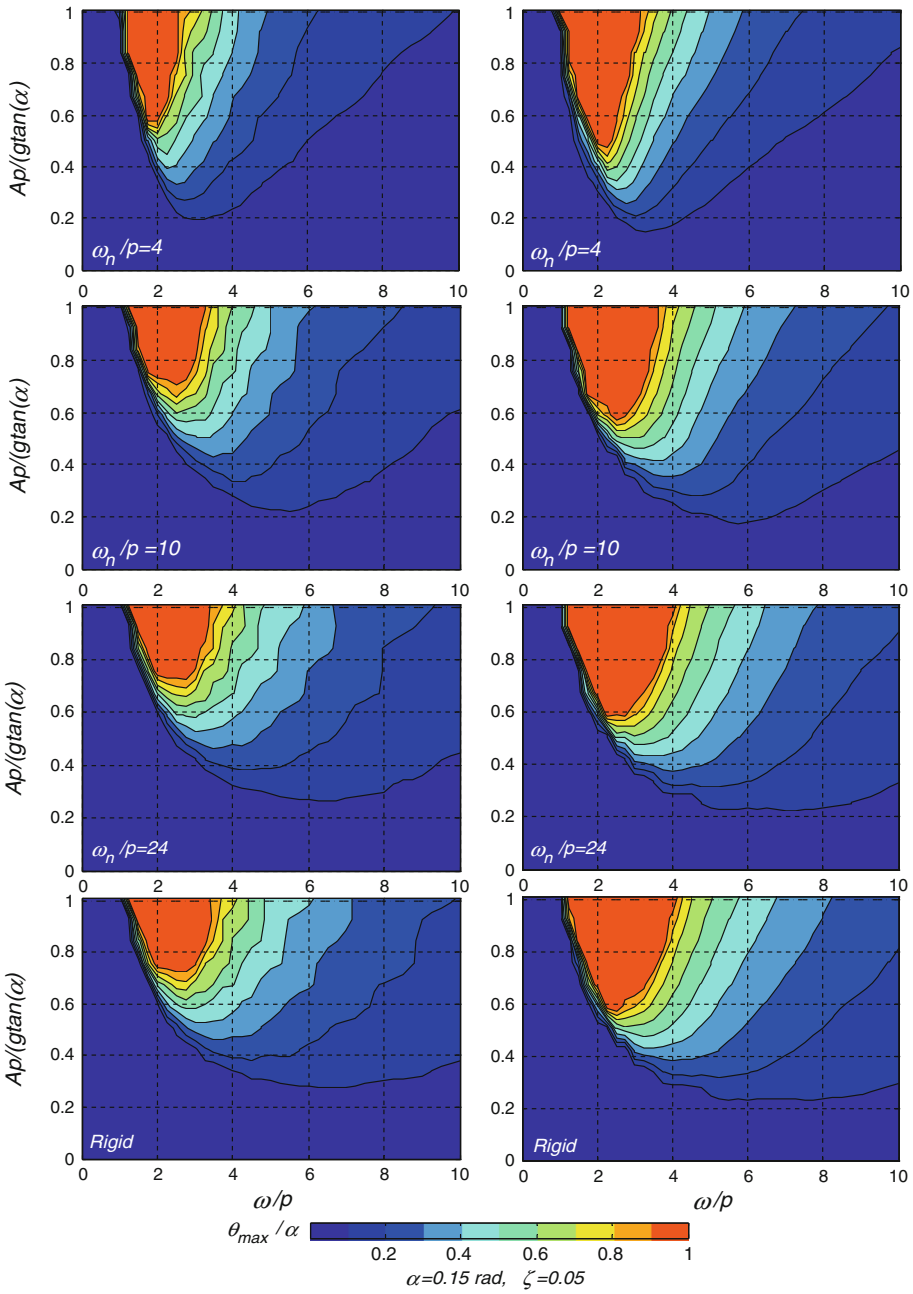

Fig. 15 Dimensionless maximum rocking demand maps for different values of relative stiffness. The contours show the median (*left column*) and maximum (*right column*) of the rocking demand (θ_{max}/α) for all of the 20 bins defined in Table 3

Equation 8 is specific to an earthquake scenario. The uncertainties associated to the knowledge of Z (A and ω in this case) can be evaluated separately, but are not considered here. Within this context, Eq. 8 can be used as a part of the probabilistic seismic demand analy-

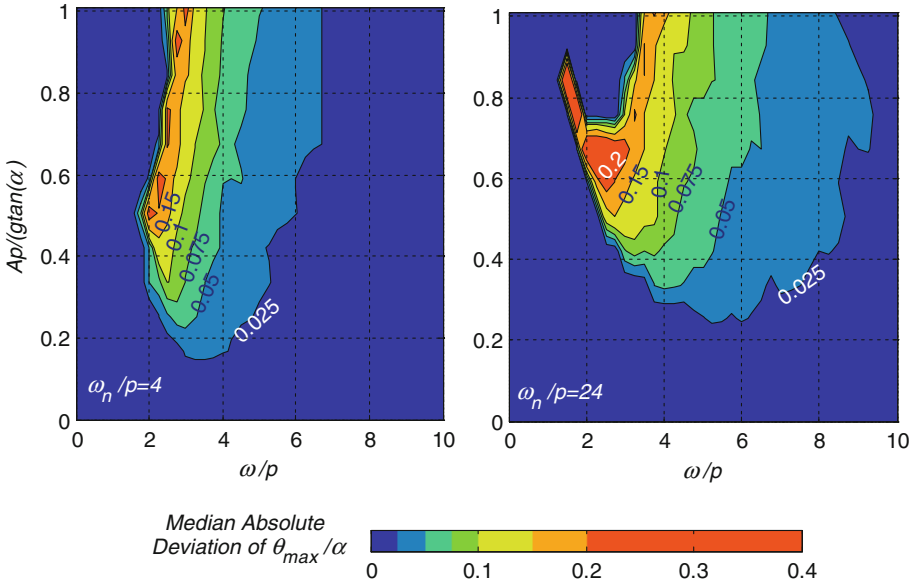

Fig. 16 Dimensionless maps of the median absolute deviation of the maximum rocking demand (θ_{max}/α) amongst all the 20 bins defined in Table 3 for two different values of relative stiffness. Note that the contours are unequally spaced

sis (PSDA) procedure. PSDA provides a framework to determine the exceedance rate of an engineering design parameter (EDP) above a certain threshold value. To do this, numerous earthquake scenarios are considered and the probability that the design parameter will exceed the threshold under any given scenario is evaluated (see Sehhati 2008 and the references therein). The computation of Eq. 8 would be integral in assessing the contribution of a subset of pulse-type earthquake scenarios which display forward directivity to determine the exceedance rate of the EDP.

Equation 8 can be computed by formulating statistical relationships between the EDP $\theta_{\max}/\alpha$ and descriptive IMs that relate to pulse intensity parameters such as T_p. An attempt to qualitatively correlate the maximum rocking response to different IMs presented several challenges (see Sect. 3.1.2). While using vector valued IMs could be an effective solution to these challenges, this approach would necessitate the evaluation of a large sample of forward directivity records and the current database of forward directivity records might not be adequate. An alternative approach, proposed by Sehhati (2008), proposes the use of wavelets as unique descriptors of pulse-type ground motions and structural response is estimated using conventional time domain analyses. However, this approach does not consider the effect of pulse shape parameters on response. Using the binning described in 3.2.3, this probabilistic approach is extended to include the effect of pulse shape parameters on the demand parameter.

Pulse period and amplitude can be estimated through the use of empirical relationships for records which display forward directivity and these parameters can be used interchangeably with A and ω. However, no deterministic methods exist for estimating pulse shape parameters (see Sect. 3.2.3). Pulse shape parameters are independent of magnitude or distance to the causative fault and relate to fault asperities, which are not explicitly considered in probabilistic analyses. Halldorsson et al. (2011) have proposed a statistical approach which assigns

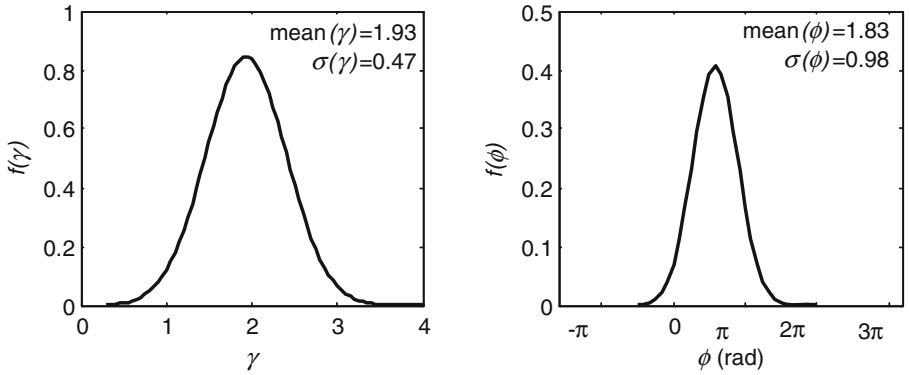

Fig. 17 Probability density functions of the parameters controlling the shape of the M&P wavelet (data from Halldorsson et al. 2011)

the independent parameters γ and ϕ a Gaussian probability distribution based on available forward directivity ground motions. These relationships, presented in Fig. 17, will be used in this paper to take the effect of pulse shape into account. Using this information, Eq. 8 can be rewritten as:

$$\lambda_{scenario,pulse}(x) = \int_{\gamma_0}^{\gamma_f}\int_{\phi_0}^{\phi_f} P\left((\theta_{\max}/\alpha)_{scenario,pulse} > x|A,\omega,\gamma,\phi\right) f(\gamma) f(\phi) d\gamma d\phi \quad (9)$$

where (γ_0, ϕ_0) and (γ_f, ϕ_f) represent the lower and upper bounds of realistic pulse shape parameters. The probability term $P((\theta_{\max}/\alpha)_{scenario,pulse} > x|A,\omega,\gamma,\phi)$ denotes the probability that a parameter x will be exceeded when all pulse parameters are known. $f(\gamma)$ and $f(\phi)$ are the probability density functions presented in Fig. 17. For computational ease, the double integral in Eq. 10 can be expressed as a discrete sum. As was done in Sect. 3, ground motion bins can be assumed to be representative for ranges of γ and ϕ. Equation 9 simplifies to:

$$\lambda_{scenario,pulse}(x) = \sum_{Bin} P((\theta_{\max}/\alpha)_{scenario,pulse,bin} > x|A,\omega,Bin) P(Bin) \quad (10)$$

where the probability of $\theta_{\max}/\alpha$ exceeding a threshold x for a given scenario and a bin is presented by $P((\theta_{\max}/\alpha)_{scenario,pulse,bin} > x|A,\omega,Bin)$, and $P(Bin)$ is the cumulative probability of occurrence of the given bin. $P(Bin)$is calculated using the lower and upper bound values for γ and ϕ specified in Table 3, and using the independent probability distributions provided in Fig. 17:

$$P(Bin) = \int_{\gamma,bin,0}^{\gamma,bin,f} f(\gamma)d\gamma \int_{\phi,bin,0}^{\phi,bin,f} f(\phi)d\phi \quad (11)$$

where $\gamma_{bin,0}, \gamma_{bin,f}, \phi_{bin,0}$ and $\phi_{bin,f}$ denote the range of pulse shape parameters pertaining to a specific bin (see Table 3). Using a similar method as Sehhati (2008), $P((\theta_{\max}/\alpha)_{scenario,pulse,bin} > x|A,\omega,Bin)$ in Eq. 10 is replaced by a Heaviside function $H(y)$, which ensures that only bins which contribute to the probability of exceedance are considered:

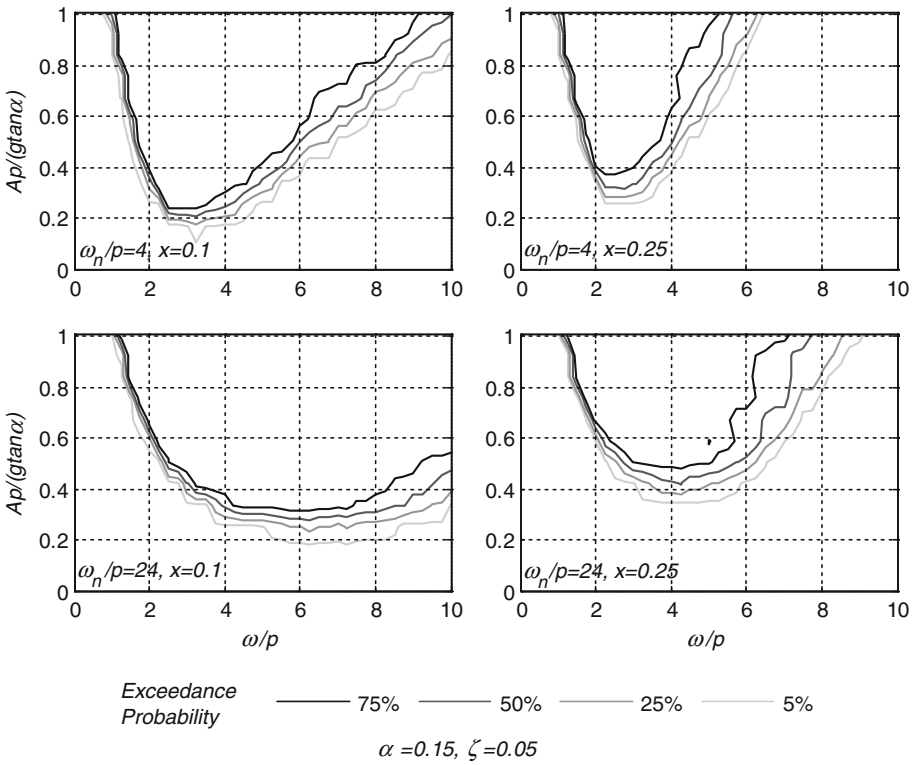

Fig. 18 Dimensionless intensity maps for different values of relative stiffness and different values of the threshold parameter, x. The contour lines depict the borders of regions where a certain exceedance probability is observed amongst all ground motion bins

$$\lambda_{scenario,pulse}(x) = \sum_{Bin} H((\theta_{\max}/\alpha)_{scenario,pulse,bin}(A,\omega) - x)P(Bin) \qquad (12)$$

For the structure investigated (with specified ω_n, p, α, ζ), dimensionless demand maps can be created for each bin and used to evaluate $H(y)$ in Eq. 12 for the pertinent values of A and ω.

Figure 18 presents the results visually through dimensionless demand maps in which the contour lines identify the pulse intensity parameters where a specific probability of exceedance is observed. Two different values of relative stiffness are considered ($\omega_n/p = 4$, 24), along with two different values of the threshold parameter ($x = \theta_{max}/\alpha = 0.1, 0.25$).

The results presented in Fig. 18 can be conveniently used in a probabilistic seismic demand analysis framework for cases where a pulse with given intensity parameters (A, ω) can be predicted due to directivity effects. This method accounts for a wide range of permissible pulse shape parameters, therefore addressing an important limitation of utilizing recorded ground motion accelerograms. It is also important to note that for rocking structures there are no established methods for ground motion selection to be used in PSDA analyses. Alternatively, more accurate results may be obtained from Monte Carlo simulation using many synthetic near-field ground motion records which account for the whole range of pulse shape parameters. Such an approach was recently followed by Psycharis et al. (2013), who investigated the seismic response of classical columns in the near-field using a PSDA framework. However,

dimensionless demand maps can provide valuable understanding of the rocking amplification at a smaller computational cost. A limitation of this methodology is that it assumes that the response to fitted wavelets is an ideal descriptor of maximum rocking amplitude. Although velocity pulses are good descriptors for large rocking structures, there are limitations to pulse-based analyses, as discussed in Sect. 3.3.3. For a more thorough analysis, a statistical evaluation of the quality of fit of pulses to the response of pulse-type records is required. While the consideration of vertical ground motions is beyond the scope of the current paper, their high frequency content would have little direct influence on the rocking amplitude of large structures. However, vertical ground motions may influence uplift and change rocking amplification patterns and therefore have an appreciable indirect effect.

4.2.2 Non-pulse type records

The response to non-pulse type records is governed by the interaction of short duration acceleration pulses. Therefore the response is significantly dependent on the magnitude, spacing and duration of these random pulses. Some IMs, such as PGV, have the potential to be used in ground motion selection (Sorrentino et al. 2006) although further work may be required to assert the 'efficiency' of the IM (Luco and Cornell 2007). Instead, a reliable and unbiased stochastic earthquake generation method may be utilized to treat the problem with time domain analyses (Bazzurro et al. 2004).

Through the use of a simple earthquake generation method, based on a limited number of parameters such as earthquake magnitude and distance to the causative fault, the response to non-pulse type earthquakes can be investigated with multiple nonlinear dynamic analyses within a PSDA framework. Typically, the rocking response to non-pulse type earthquakes is expected to be small. However, in the near-field of large earthquakes where significant low frequency content is observed, high rocking amplitudes could be experienced. In the far-field, where pulses are unlikely, the effect of non-pulse type motions will be dominant. Subsequently, combining the results for pulse-type and non-pulse type earthquake scenarios would allow a general determination of the rate of exceedance of a given maximum rocking amplitude (Tothong et al. 2007).

5 Conclusions

In this paper, the rocking response of large structures to pulse-type earthquake records was characterized and quantified with the use of a lumped mass structural model rocking on rigid ground. The idealization of pulse-type records with fitted wavelets allowed quantification of the dominance of the earthquake pulse for structures of varying scale and stiffness. Through the use of physical similarity, it was shown that earthquakes with different pulse intensities but similar pulse shapes result in matching response spectra when appropriate dimensionless parameters are defined. This demonstrates that velocity pulses are good descriptors of pulse-type earthquakes in many cases. Further, comparison of the maximum rocking response to different pulse-type records and their fitted wavelets resulted in reasonable agreement. The accuracy and the limitations of utilizing wavelets instead of pulse-type records were discussed in detail.

To propose a predictive framework based on fitted velocity wavelets, a further understanding of how pulse parameters affect the response was required. Quantification of the effect of the pulse parameters on the response showed that pulse shape can significantly affect maximum rocking demand. Visualization of results through dimensionless demand

maps enabled depiction of the maximum rocking response for a wide range of structures and intensities in a condensed manner. Finally, a probabilistic method was proposed to estimate maximum rocking under the influence of pulse-type earthquakes with known pulse intensities, while considering the effect of pulse shape parameters on the response. This method, when combined with probabilistic seismic demand analysis, may have predictive power in the near-field.

Acknowledgments Funding for this research was provided by Trinity College, Cambridge Overseas Trust and the Suna and Inan Kirac Foundation. The authors would like to thank Dr. Benedikt Halldorsson, Dr. George Mavroeidis and Dr. Adrian Rodriguez-Marek for their valuable suggestions regarding use of wavelets for the simulation of pulse-type ground motions. Useful reviewer feedback is also appreciated.

References

Abrahamson NA, Silva WJ (1997) Empirical response spectral attenuation relations for shallow crustal earthquakes. Seismol Res Lett 68(1):94–127

Acikgoz S, DeJong MJ (2012) The interaction of elasticity and rocking in flexible structures allowed to uplift. Earthq Eng Struct Dyn 41(15):2177–2194

Acikgoz S, DeJong MJ (2013) Analytical and experimental observations on vibration modes of flexible rocking structures. Society for earthquake and civil engineering dynamics (SECED) young engineer's conference, Newcastle, UK

Ambraseys NN, Smit P, Douglas J et al (2004) Internet site for European strong-motion data. Bollettino di Geofisica Teorica e Applicata 45(3):113–129

Anderson JC, Bertero VV (1987) Uncertainties in establishing design earthquakes. J Struct Eng 113(8):1709–1724

Apostolou M, Gazetas G, Garini E (2007) Seismic response of slender rigid structures with foundation uplifting. Soil Dyn Earthq Eng 27(7):642–654

Aslam M, Scalise DT, Godden WG (1980) Earthquake rocking response of rigid bodies. J Struct Div 106(2):377–392

Baker JW (2007) Quantitative classification of near-fault ground motions using wavelet analysis. Bull Seismol Soc Am 97(5):1486–1501

Bazzurro P, Sjoberg B, Luco N (2004) Post-elastic response of structures to synthetic ground motions. Report for Pacific Earthquake Engineering Research (PEER) Center Lifelines Program Project 1G00 Addenda. CA (US), pp 65–112

Beck JL, Skinner RI (1973) The seismic response of a reinforced concrete bridge pier designed to step. Earthq Eng Struct Dyn 2(4):343–358

Bray JD, Rodriguez-Marek A (2004) Characterization of forward-directivity ground motions in the near-fault region. Soil Dyn Earthq Eng 24(11):815–828

Chiou B, Darragh R, Gregor N et al (2008) NGA project strong-motion database. Earthq Spectra 24(1):23–44

DeJong MJ (2012) Amplification of rocking due to horizontal ground motion. Earthq Spectra 28(4):1405–1421

Halldorsson B, Mavroeidis GP, Papageorgiou AS (2011) Near-fault and far-field strong ground-motion simulation for earthquake engineering applications using the specific barrier model. J Struct Eng 137(3):433–444

Housner GW (1963) The behaviour of inverted pendulum structures during earthquakes. Bull Seismol Soc Am 53(2):403–417

Huckelbridge AA, Clough RW (1978) Seismic response of uplifting building frame. J Struct Div 104(8):1211–1229

Luco N, Cornell CA (2007) Structure-specific scalar intensity measures for near-source and ordinary earthquake ground motions. Earthq Spectra 23(2):357–392

Makris N, Roussos YS (2000) Rocking response of rigid blocks under near-source ground motions. Geotechnique 50(3):243–262

Makris N, Vassiliou MF (2012) Planar rocking response and stability analysis of an array of free-standing columns capped with a freely supported rigid beam. Earthq Eng Struct Dyn 42(3):431–449

Mavroeidis GP, Papageorgiou AS (2003) A mathematical representation of near-fault ground motions. Bull Seismol Soc Am 93(3):1099–1131

Mavroeidis GP, Dong G, Papageorgiou AS (2004) Near-fault ground motions, and the response of elastic and inelastic single-degree-of-freedom (SDOF) systems. Earthq Eng Struct Dyn 33(9):1023–1049

Meek JW (1975) Effects of foundation tipping on dynamic response. J Struct Div 101(7):1297–1311

Meek JW (1978) Dynamic response of tipping core buildings. Earthq Eng Struct Dyn 6(5):437–454
Psycharis IN (1983) Dynamics of flexible systems with partial lift-off. Earthq Eng Struct Dyn 11(4):501–521
Psycharis IN, Fragiadakis M, Stefanou I (2013) Seismic reliability assessment of classical columns subjected to near-fault ground motions. Earthq Eng Struct Dyn. doi:10.1002/eqe.2312
Rathje EM, Abrahamson NA, Bray JD (1998) Simplified frequency content estimates of earthquake ground motions. J Geotech Geoenviron Eng 124(2):150–158
Sehhati R (2008) Probabilistic seismic demand analysis for the near fault zone. Washington State University, dissertation
Sharpe RD, Skinner RI (1983) The seismic design of an industrial chimney with rocking base. Bull N Z Natl Soc Earthq Eng 16(2):98–106
Sorrentino L, Masiani R, Decanini LD (2006) Overturning of rocking rigid bodies under transient ground motions. Struct Eng Mech 22(3):293–310
Tothong P, Cornell CA, Baker JW (2007) Explicit directivity-pulse inclusion in probabilistic seismic hazard analysis. Earthq Spectra 23(4):867–891
Trifunac MD, Brady AG (1975) A study on the duration of strong earthquake ground motion. Bull Seismol Soc Am 65(3):581–626
Vassiliou MF, Makris N (2011) Estimating time scales and length scales in Pulselike earthquake acceleration records with wavelet analysis. Bull Seismol Soc Am 101(2):596–618
Yim CS, Chopra AK (1984a) Dynamics of structures on two-spring foundation allowed to uplift. J Eng Mech 110(7):1124–1146
Yim CS, Chopra AK (1984b) Earthquake response of structures with partial uplift on Winkler foundation. Earthq Eng Struct Dyn 12(2):263–281
Yim CS, Chopra AK (1985) Simplified earthquake analysis of multistory structures with foundation uplift. J Struct Eng 111(12):2708–2731
Yim CS, Chopra AK, Penzien J (1980) Rocking response of rigid blocks to earthquakes. Earthq Eng Struct Dyn 8(6):565–587
Zhang J, Makris N (2001) Rocking response of free-standing blocks under cycloidal pulses. J Eng Mech 127(5):473–483